

## **Section 1**

**Atmospheric data assimilation  
schemes, analysis and initialization,  
data impact studies, observing system  
experiments**



## **Operational implementation of flow-dependent background error correlations at Météo-France using a wavelet model and ensemble data assimilation**

Loïk Berre, Gérald Desroziers, Hubert Varella  
CNRM-GAME, Météo-France and CNRS  
42 avenue Coriolis 31057 Toulouse, France  
loik.berre@meteo.fr

Assimilation of observations in numerical weather prediction systems relies on modelling of forecast error spatial correlations. These correlations allow observed information to be spatially filtered and propagated during the analysis process.

A new model of these correlations is now used operationally at Météo-France, in order to take into account their flow dependence. This approach is based on a wavelet representation of geographical variations of correlations (Fisher 2003, Varella et al 2011). It relies also on the 6 members of the ensemble data assimilation system (Berre and Desroziers 2010), which are sampled in a sliding way over the last 4 current days. This provides a set of 96 perturbed forecasts, from which error correlations can be estimated in a robust way.

Figure 1 shows geographical variations of horizontal correlation length-scales, estimated for the period 24-27 February 2010. Short length-scales are observed in the vicinity of low pressure areas in the Eastern part of USA and over Northern Atlantic and Europe. This allows small scale structures that are observed in these regions to be better described.

In the context of the implementation of a new computer, it is planned in the future to increase the ensemble size. This will allow variability of error structures from one day to the other to be represented, and ensemble predictions to be better initialized.

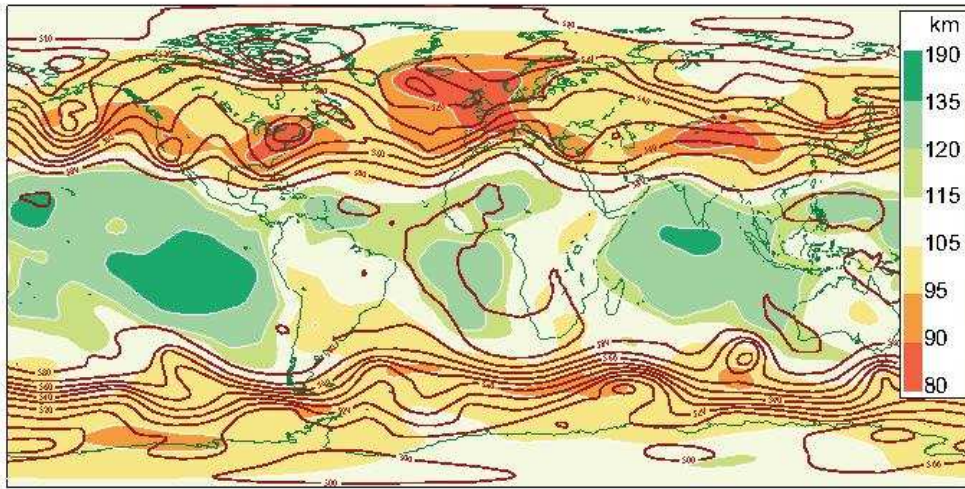


Figure 1 : Horizontal length-scales of background error correlations for wind near 500 hPa (shaded, in km), averaged over the period from 24 February 2010 00 UTC to 27 February 2010 18 UTC, and superimposed to the 500 hPa geopotential field (contours, dam) valid on 26/02/2010 00UTC. The length-scale of a local correlation function is a measure of its spatial extension.

### References :

Berre, L. and G. Desroziers, 2010: Filtering of Background Error Variances and Correlations by Local Spatial Averaging: A Review. *Mon. Wea. Rev.*, 138, 3693-3720.

Fisher, M., 2003: Background error covariance modeling. *Proc. ECMWF Seminar on "Recent Developments in Data Assimilation for Atmosphere and Ocean"*, 8-12 Sept 2003, Reading, U.K., 45-63.

Varella, H., Berre, L. and Desroziers, G. (2011), Diagnostic and impact studies of a wavelet formulation of background-error correlations in a global model. *Q.J.R. Meteorol. Soc.*, 137: 1369–1379. doi: 10.1002/qj.845

# Assessing the impact of the SAPHIR microwave sounder on board Megha-Tropiques into the ARPEGE global model

Philippe Chambon, Louis-François Meunier, Frank Guillaume and Jean-François Mahfouf  
CNRM-GAME, Météo-France and CNRS  
42 avenue Coriolis 31057 Toulouse, France  
[philippe.chambon@meteo.fr](mailto:philippe.chambon@meteo.fr)

The Megha-Tropiques satellite is a joined Indo-French mission (CNES/ISRO) dedicated to the study of the water cycle and energy budget in Tropical regions. The core payload is composed by three radiometric instruments, amongst which, the microwave sounder SAPHIR. With six channels, SAPHIR provides information on atmospheric water vapour at different altitudes. The main original feature of Megha-Tropiques is to provide observations with a high time frequency thanks to its orbit that makes a slight angle with the Earth's equatorial plane. Therefore it is possible to observe a given area over the Tropics 3 to 6 times per day. In consequence, the number of humidity observations provided by microwave instruments is significantly increased along the Tropical belt.

Figure 1 illustrates the large fraction of the Tropics, which is observed during a 6-hour assimilation window. One can also see on Figure 1 that the main characteristics of the water vapour field observed with SAPHIR (Figure 1-(a)), such as dry air areas over South America and the Southern Pacific Ocean (red areas), are also present in the ARPEGE 6-hour forecast (Figure 1-(b)). Large discrepancies can also be noticed between observed and simulated brightness temperatures in rainy areas (blue areas), like for the mesoscale convective systems crossing West Africa. Indeed the use of observations, in cloudy and rainy systems, is more challenging than in clear sky conditions and are not simulated nor assimilated yet within the ARPEGE operational forecasting system.

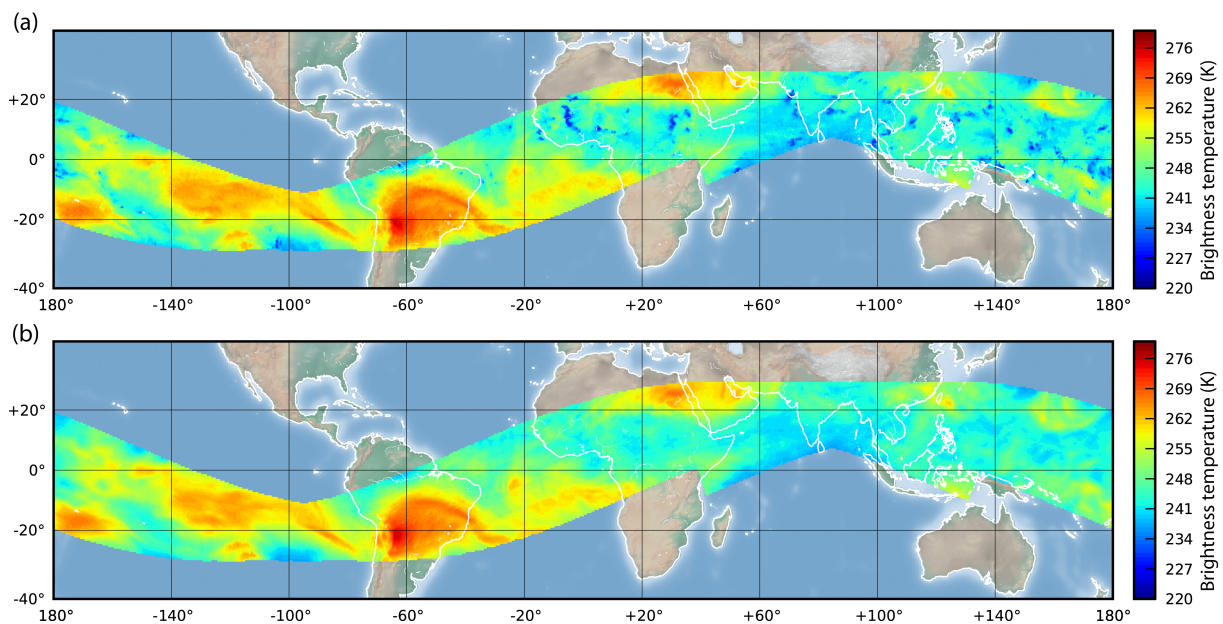


**Figure 1: SAPHIR observations (a) and model simulated (b) brightness temperatures at 183.1 +/- 1.1 GHz for the ARPEGE 6-hour assimilation window on July 2<sup>nd</sup>, 2012 at 0h00 UTC.**

The SAPHIR brightness temperatures have been assimilated in a recent version of the ARPEGE 4D-Var assimilation system over a two-month period in Summer 2012

(experiment noted EXP below); its impact is assessed compared to an experiment only monitoring SAPHIR (noted CTRL below). Figure 2-(a) shows the better agreement of model simulated brightness temperatures and observations that can be noted in the EXP with respect to the CTRL experiment, for SAPHIR observations and MHS on board MetOp-A. A similar improvement of innovation statistics was also found for other microwave sounders such as AMSU-B on board NOAA-18 or MHS on board NOAA-19, as well as for Infrared water vapour channels of SEVIRI/Meteosat-10 or HIRS/MetOp-A (not shown). These improvements in the EXP experiment with respect the CTRL experiment demonstrate the positive synergy of Megha-Tropiques data with the present observing system.

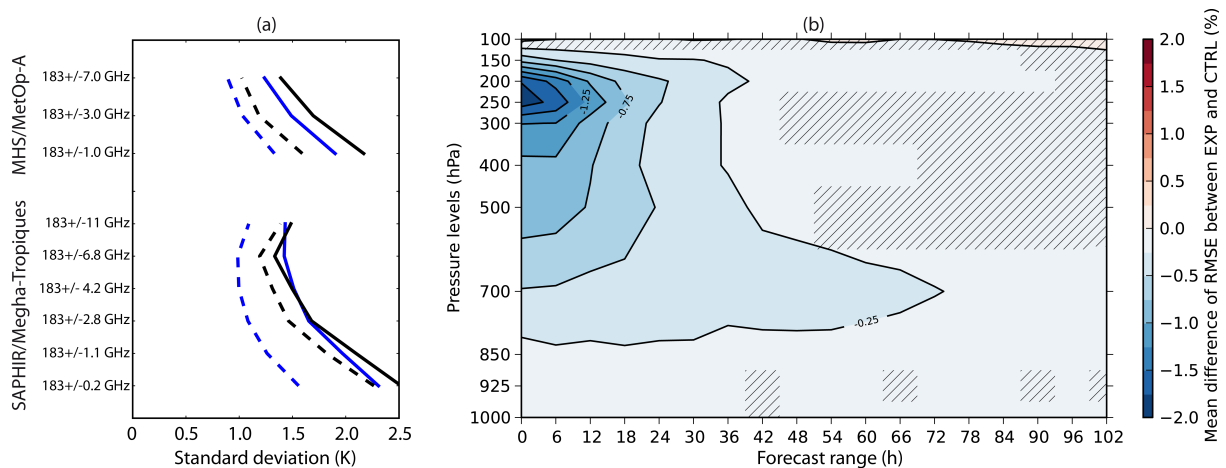


**Figure 2: (a) Standard deviation of first guess departures (full lines) and of analysis departures (dashed lines) for the CTRL (black lines) and the EXP experiments (blue lines) over the tropical band, for SAPHIR and MHS/MetOp-A. (b) Difference of Root Mean Square Error between the EXP and the CTRL experiments compared to ECMWF analysis as function of forecast range. An improvement in the EXP experiment corresponds to a negative difference of RMSE. Areas that are not dashed indicate differences of RMSE which are significant at the 99% level of confidence.**

In order to evaluate differences in the EXP and the CTRL model forecasts, relative humidity fields are compared with ECMWF operational analyses which are used on a regular grid of  $1.5^\circ$ . The comparison reveals that the most significant improvement can be found during the first 12 hours of forecast between 400 and 150hPa (Figure 2-(b)); it represents a relative decrease of roughly 10% of the RMSE between the CTRL and the ECMWF analysis. A statistically significant impact can also be seen up to 72 hours of forecast between 800 and 700hPa but represent a smaller relative reduction of the RMSE of the CTRL, between 1% and 2%. This improvement up to 72 hours at 700 hPa can also be identified by comparisons with radiosonde data, with a similar magnitude of 1% to 2% (not shown).

Plans are made to assimilate SAPHIR data in a future version of the Météo France operational global forecasting system ARPEGE, as well as in the four regional models ALADIN along the Tropical belt covering French Overseas Territories. More details on SAPHIR data impact evaluation can be found in Chambon et al. (2014).

### Reference:

Philippe Chambon, Louis-François Meunier, Frank Guillaume, Jean-Marcel Piriou, Rémy Roca and Jean-François Mahfouf, 2014: Investigating the impact of the water vapour sounding observations from SAPHIR on board Megha-Tropiques into the ARPEGE global model (In preparation for Q. J. R. Meteorol. Soc.)

## Assimilation of GCOM-W1/AMSR2 radiance data into JMA's NWP systems

Masahiro Kazumori\* and Takumu Egawa

Numerical Prediction Division, Forecast Department, Japan Meteorological Agency

\*Corresponding author: M. Kazumori, JMA, Otemachi, Chiyoda-ku, Tokyo, 100-8122, Japan

E-mail: kazumori@met.kishou.go.jp

The Japan Meteorological Agency (JMA) develops and operates global and mesoscale numerical weather prediction (NWP) systems for weather forecasting. Japan suffers annually from heavy precipitation caused by typhoons and seasonal fronts, and the main source of this precipitation is moisture from oceans. Against such a background, the use of satellite observations (especially moisture-sensitive data such as microwave imager radiance data) is crucial in analysis conducted with JMA's NWP systems for the production of accurate initial conditions. Clear sky radiance data from microwave imagers are assimilated in JMA's global NWP system. In the Agency's mesoscale NWP system, clear sky radiance data and precipitation retrievals from microwave imagers are assimilated.

Although the temporal frequency of data from polar-orbiting satellites is insufficient for use in operational regional models, data from multiple satellites can be used to fill temporal and spatial gaps in data assimilation. Frequent analysis updates with multiple satellite observations can reflect rapidly changing humidity distribution to initial NWP fields. The Global Change Observation Mission 1st – Water (GCOM-W1)/Advanced Microwave Scanning Radiometer 2 (AMSR2) imager was launched in May 2012 by the Japan Aerospace Exploration Agency (JAXA) as a successor to the Advanced Microwave Scanning Radiometer for Earth Observing System (AMSR-E). AMSR2 has an afternoon orbit (known as the A-Train), and the equator crossing time in its ascending orbit is approximately 1:30 p.m. local time. AMSR2 radiance data have been assessed in JMA's NWP systems.

Although AMSR2 radiance data have large biases compared to AMSR-E data, most of the biases are considered to be constants in space and time and are without scene dependency. The quality of bias-corrected AMSR2 radiance data is comparable to that of data from AMSR-E and other microwave imagers. To investigate the related impact on analysis and forecasts in data assimilation experiments, AMSR2 radiance data were incorporated in addition to the currently used microwave imager data from the Defense Meteorological Satellite Program (DMSP)/Special Sensor Microwave Imager Sounder (SSMIS) F16, F17, F18, and Tropical Rainfall Measuring Mission (TRMM)/TRMM Microwave Imager (TMI).

Experiments with JMA's global NWP system demonstrated improvement in humidity fields. Figure 1 shows the results of verification for humidity analysis and forecast fields against radiosonde observations in the Southern Hemisphere. In experiments with JMA's mesoscale NWP system, increases in the analysis increment of humidity with AMSR2 radiance data assimilation were found. These resulted in significant improvement of precipitation forecasts

(Fig. 2). Based on these findings, AMSR2 radiance data were assimilated into JMA's NWP systems on 12 September 2013. Further work in the field will involve the inclusion of future microwave imager data (e.g., from the Global Precipitation Measurement (GPM) Microwave Imager) and the development of an all-sky radiance assimilation system in JMA'S systems.

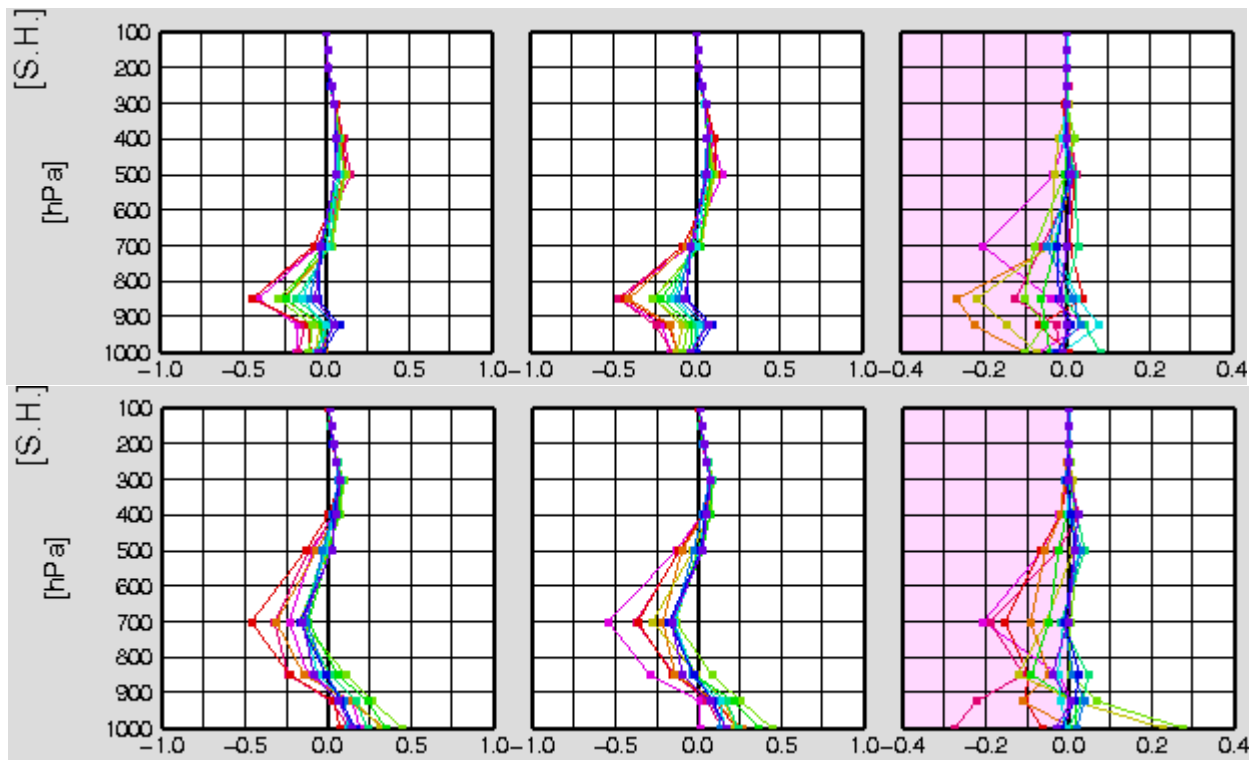


Fig. 1. Specific humidity field verification for the Southern Hemisphere against radiosonde observation for different forecast times (FT) [hours]. The upper panels show the results from experiments for August 2012 using JMA's global NWP system. The lower panels show the results for January 2013. The panels on the left show the bias error of the test run (with AMSR2) and the middle panels show that of the control run (without AMSR2). The panels on the right indicate root mean square error differences between the test run and the control run for forecast times. The unit is g/kg.

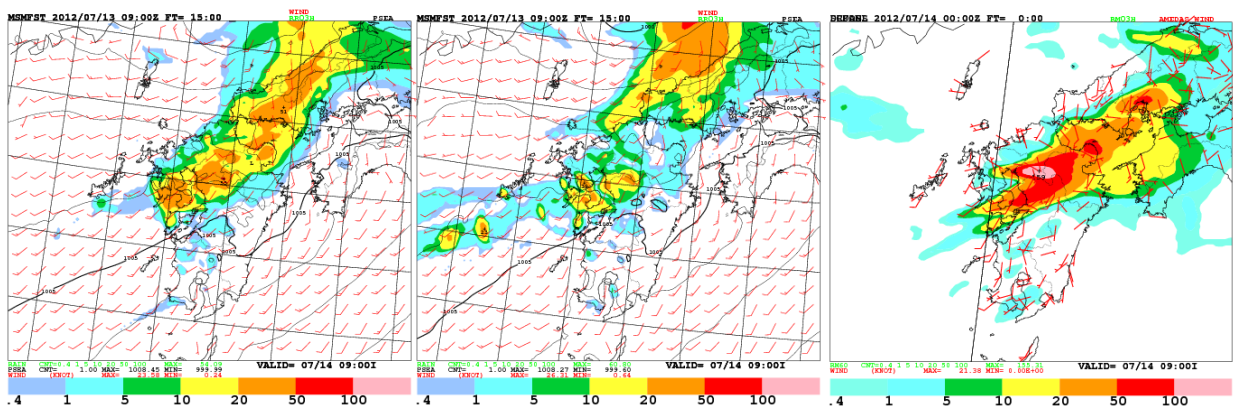


Fig. 2. Comparison of three-hour cumulative rainfall forecasts for 00 UTC on July 14 2012. The forecast period is 15 hours. The panel on the left shows the results of the test run (with AMSR2), the middle panel shows those of the control run (without AMSR2) and the panel on the right shows rainfall distribution estimated from radar observations and rain gauges. The unit is mm/3 hr.

# Data assimilation experiments for tropical cyclones with the NHM-LETKF

Masaru Kunii<sup>1</sup>

<sup>1</sup>Forecast Research Department, Meteorological Research Institute

Forecasts for tropical cyclones (TCs) have been one of the most important issues from the view point of mitigating natural disasters. Although TC track forecasts have constantly improved over the past several decades owing to advances in numerical weather prediction (NWP) models as well as observational capabilities (Rappaport et al. 2009), improving TC intensity has still been a challenging task. One of the major difficulties in simulating TC intensity is the lack of observations over the ocean, especially near TCs. As compensation of real observations, a TC bogus method has been utilized to modify TC structures in initial conditions, leading to improvement of TC forecasts. However, because the typical structure is assumed in the bogus scheme, the discrepancy between actual TCs and these artificial data may become large, especially in the generation and extra-tropical transition stages of TCs.

In the current study, motivated by Chen and Snyder (2007), assimilation of TC position and intensity information is applied with a realistic NWP model. Although many studies have been published thus far investigating the impacts of best track estimates of TC minimum central pressure and position, so-called TC Vital observations (Torn and Hakim 2009; Torn 2010; Hamill et al. 2011), the comparison of the TC Vital data with different assimilation methods has not been performed. Here, impacts of the TC Vital data are evaluated through sensitivity experiments with different assimilation strategies. For data assimilation experiments, the NHM-LETKF system (Kunii 2013) is utilized with almost similar configurations of the literature.

Throughout the following sensitivity experiments, TC Vital data with large difference from the first guess field are assimilated so as to emphasize the impact of the data. Compared with the TC intensity and position represented in the first guess field, the minimum central pressure and central position of the TC Vital are deeper by 16 hPa, and located 100 km west from the first guess, respectively. First, the impact of the different assimilation strategies is examined. When the data are assimilated as a surface pressure observation, unnatural pressure pattern emerges near the TC center in the analysis (Fig. 1a). This is probably due to the large discrepancy of the TC positions in the first guess field and the assimilated observation. By contrast, assimilating TC position and intensity improves the sea level pressure field with reasonable analysis increments (Fig. 1b).

Next, in order to show the individual impact of the intensity and position information, the TC minimum central pressure and position data are separately assimilated. Figure 2 shows the analysis increments of surface pressure fields in each experiment. When the TC minimum central pressure information is assimilated, the intensity becomes closer to the observation although relatively small positive increments appear near the center of TC. With TC position information, positive and negative increments emerge east and west side of the TC center in the first guess. This increment pattern implies the relocation of the TC position, indicating the assimilation works as expected.

---

<sup>1</sup> *Corresponding author address:* Masaru Kunii, Forecast Research Department, Meteorological Research Institute, Tsukuba, Ibaraki 305-0052, JAPAN.  
E-mail: [mkunii@mri-jma.go.jp](mailto:mkunii@mri-jma.go.jp)

In the current study, the impact of the TC Vital data is evaluated through sensitivity experiments. Besides further comparison of TC Vital with TC bogus data, exploration of new assimilation strategies of TC Vital would be a future subject.

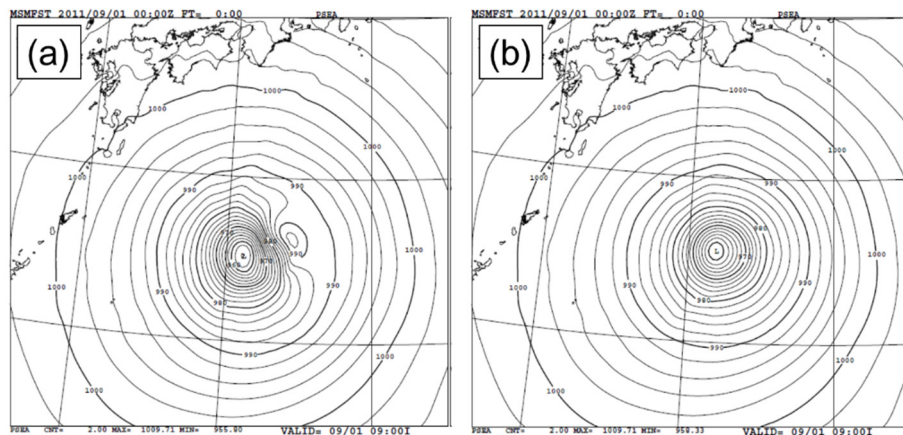


FIG. 1. Analyzed sea level pressure (hPa) when TC Vital data are assimilated (a) as a surface pressure observation, (b) as position and intensity information.

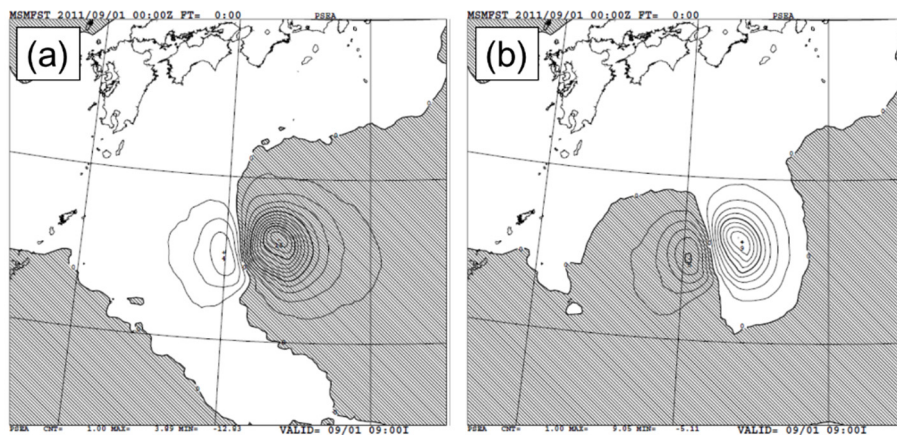


FIG. 2. Analysis increments of mean sea level pressure (hPa) when (a) TC intensity, (b) TC position information is assimilated. Shade color shows negative analysis increments.

## References

- Chen, Y., and C. Snyder, 2007: Assimilating vortex position with an ensemble Kalman filter. *Mon. Wea. Rev.*, **135**, 1828–1845.
- Hamill, T. M., J. S. Whitaker, M. Fiorino, and S. G. Benjamin, 2011: Globalensemble predictions of 2009's tropical cyclones initialized with an ensemble Kalman filter. *Mon. Wea. Rev.*, **139**, 668–688.
- Kunii, M., 2013: Mesoscale data assimilation for a local severe rainfall event with the NHM-LETKF system. *Wea. Forecasting*, doi: <http://dx.doi.org/10.1175/WAF-D-13-00032.1>.
- Rappaport, E. N., and Coauthors, 2009: Advances and challenges at the National Hurricane Center. *Wea. Forecasting*, **24**, 395–419.
- Torn, R. D., 2010: Performance of a mesoscale ensemble Kalman filter (EnKF) during the NOAA High-Resolution Hurricane test. *Mon. Wea. Rev.*, **138**, 4375–4392.
- Torn, R. D., and G. J. Hakim, 2009: Ensemble data assimilation applied to RAINEX observations of Hurricane Katrina (2005). *Mon. Wea. Rev.*, **137**, 2817–2829.

## **Assimilation of new satellite observations in the Météo-France global 4D-Var data assimilation system**

J.-F. Mahfouf, N. Boullot, N. Fourrié, V. Guidard, L.-F. Meunier, P. Moll, and C. Payan  
CNRM-GAME, Météo-France and CNRS  
42 Avenue G. Coriolis, 31057 TOULOUSE, France  
jean-francois.mahfouf@meteo.fr

During the last decade, the number of observations in data assimilation has increased significantly leading to improved analyses and forecasts. This increase comes from two factors : on one hand is the availability of new measuring systems (in particular from satellites) and on the other hand is the capacity of data assimilation systems to ingest more data from existing platforms.

In July 2013, the number of observations assimilated in the Météo-France operational global four-dimensional variational data assimilation system has increased dramatically from the combined availability of three new satellites. In October 2011, the satellite « Suomi-NPP<sup>1</sup> », having onboard a microwave sounder ATMS<sup>2</sup> and an hyperspectral infra-red sounder CrIS<sup>3</sup>, was launched by the United States. The radiances from ATMS are assimilated in similar way to AMSU-A and AMSU-B/MHS instrument expect that additional quality flags have been defined thanks to the availability of all frequencies from 24 GHz to 191 GHz on the same instrument. Moreover, the instrumental noise is reduced for temperature channels by a “3x3” spatial average of the satellite pixels. Regarding CrIS, a sub-set of 43 channels among the 1305 is assimilated in clear sky conditions. In September 2012, the satellite « MetOp-B » has been launched by EUMETSAT, as a follower of « MetOp-A » that remains available. The various instruments on board MetOp-B are assimilated (AMSU-A, MHS, GRAS, ASCAT) with the exception of the infra-red HIRS sounder. At last, surface wind data from the scatterometer OSCAT<sup>4</sup> onboard the Indian satellite OCEANSAT-2 launched in 2009 are available in real time for the scientific community since the end of 2012. The winds from OSCAT are assimilated with a spatial thinning of 50 km (compared to 100 km for ASCAT) but with increased observation errors. These three instruments have produced an increase of data by a factor of 2 in the global model ARPEGE, the largest contribution is coming from the infra-red hyperspectral sounders as shown in Figure 1. Forecast sensitivity to observations based on the adjoint method with the ARPEGE model and a 24-h forecast error defined by a dry energy norm with the new system (Figure 2) reveals that the AMSU-A instruments (7 sounders on different platforms) remain the most important observing system for improving the short-range model forecast skill followed by the two IASI instruments.

---

<sup>1</sup> Suomi-NPP : US program for meteorological polar orbiting satellites

<sup>2</sup> ATMS : Advanced Technology Microwave Sounder

<sup>3</sup> CrIS : Cross-track Infra-Red Sounder

<sup>4</sup> OSCAT : OCEANSAT-2 Scatterometer

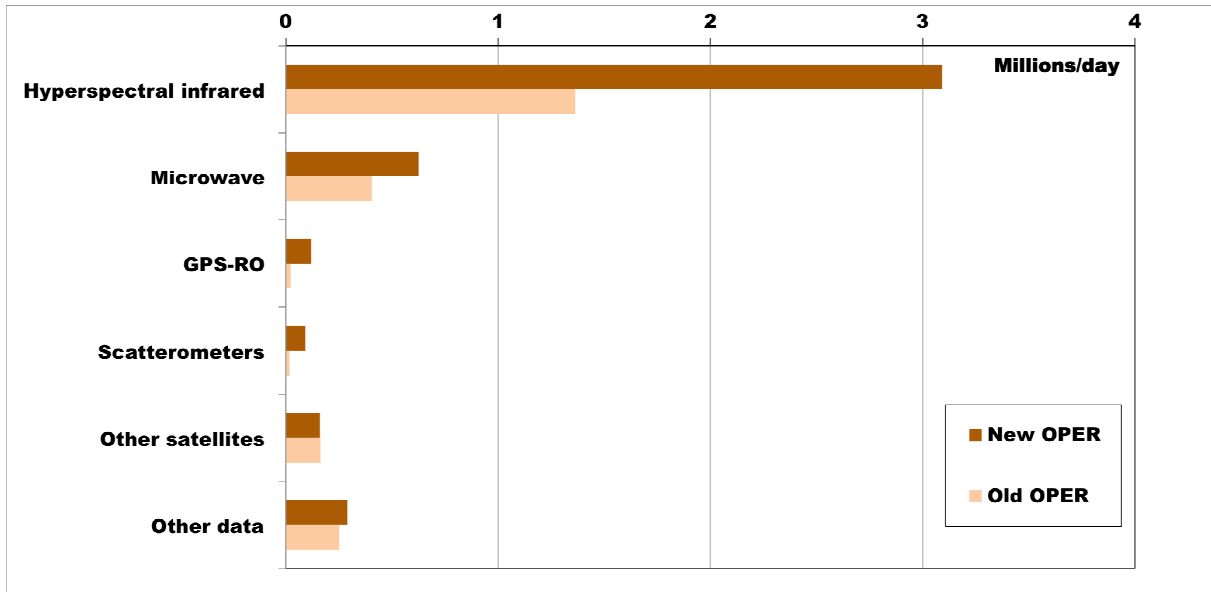


**Figure 1 :** Comparison of daily observations assimilated in the global model ARPEGE for the main observing systems (instruments onboard satellites: hyperspectral infrared sounders, microwave sounders and imagers, temperature measurements from GPS radio-occultation, surface wind measurements from scatterometers; other satellite observations; other data from radiosoundings, surface networks, aircrafts, and buoys) since the 02 July 2013 (**New OPER**) and before this date (**Old OPER**).

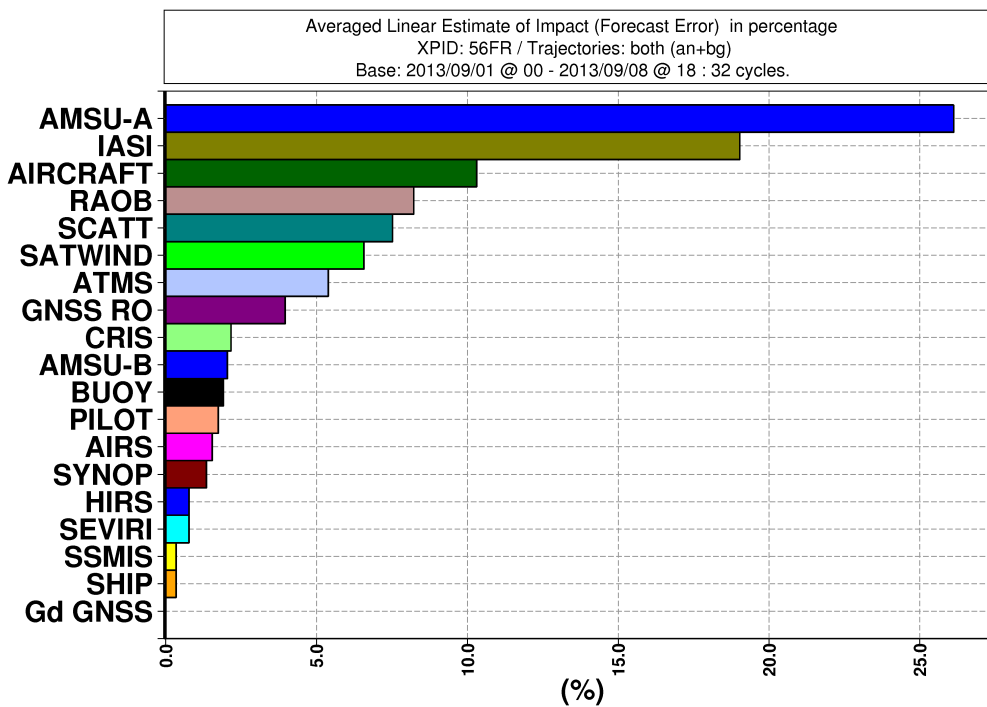


**Figure 2 :** Percentage of reduction in 24-h forecast errors (dry energy norm) in the Météo-France global model ARPEGE with the **new OPER** system (since 02 July 2013) resulting from the use of various observation types as diagnosed by the adjoint method.

# Utilization of Metop-B data in JMA's Operational Global and Mesoscale NWP Systems

Masami Moriya, Hiromi Owada, Koji Yamashita, Takumu Egawa

Numerical Prediction Division, Japan Meteorological Agency

E-mail: m.moriya@met.kishou.go.jp

## 1. Introduction

Metop is a series of three polar-orbiting meteorological satellites operated by the European Organisation for the Exploitation of Meteorological Satellites (EUMETSAT). Launched in October 2006, Metop-A is the first satellite in the series, and the Japan Meteorological Agency (JMA) has been assimilating the unit's observation data in its numerical weather prediction (NWP) systems since 2007. The current assimilation targets are Advanced Microwave Sounding Unit-A (AMSU-A), Microwave Humidity Sounder (MHS), GNSS Receiver for Atmospheric Sounding (GRAS) and Advanced Scatterometer (ASCAT) data along with one set of retrieval data (atmospheric motion vector (AMV) information) from the Advanced Very High Resolution Radiometer (AVHRR). These are useful measurements for atmospheric analysis to provide initial conditions for NWP.

Metop-B was launched in September 2012 as the second unit in the series, and became the prime operational satellite in April 2013 with Metop-A still active. JMA began assimilating data from Metop-B in addition to those from Metop-A on 28 November 2013, as Metop carries a set of heritage instruments. This report details the impacts of Metop-B data assimilation on both the global and mesoscale NWP systems.

## 2. Impacts on the global NWP system

To evaluate the quality of data from Metop-B, statistical research was performed in advance based on the mean and standard deviation of differences between the results of observation and global model simulations. The results showed that the quality of Metop-B data was comparable to that of Metop-A data, meaning that the utilization of Metop-B data increases the body of same-quality AMSU-A, MHS, GRAS, AVHRR-AMV and ASCAT data available. Accordingly, the additional use of Metop-B data into NWP systems is expected to improve analysis accuracy.

Observation system experiments were performed using the global NWP system for the one-month period of August 2013 to investigate the impacts of Metop-B data assimilation. The control experiment (CNTL) had the same configuration as the operational global system, and the additional use of Metop-B data was implemented in the test experiment (TEST). The results revealed that the assimilation of Metop-B data improved analysis and forecast fields. Figure 1 shows the outcomes of analysis and the background error of the wind speed field against radio-sonde observations in the tropics and the Southern Hemisphere. The bias at around 500 hPa in the tropics and both the bias and the root mean square error (RMSE) at around 300 hPa in the Southern Hemisphere were reduced. For other elements such as temperature and relative humidity, the bias and RMSE were slightly reduced. The quality of typhoon track predictions was improved as shown in Figure 2.

## 3. Impacts on the mesoscale NWP system

In the mesoscale NWP system, the usage of Metop data is restricted to AMSU-A and MHS. The quality of AMSU-A and MHS data from Metop-B was investigated with the mesoscale NWP system in the same way as with the global NWP system, and the results showed that data quality was also comparable to that of Metop-A (not shown). A study to determine the impacts of Metop-B data assimilation on the mesoscale NWP system was also conducted, and some forecast scores relating to precipitation and elements such as temperature and wind vectors were found to be almost neutral (not shown).

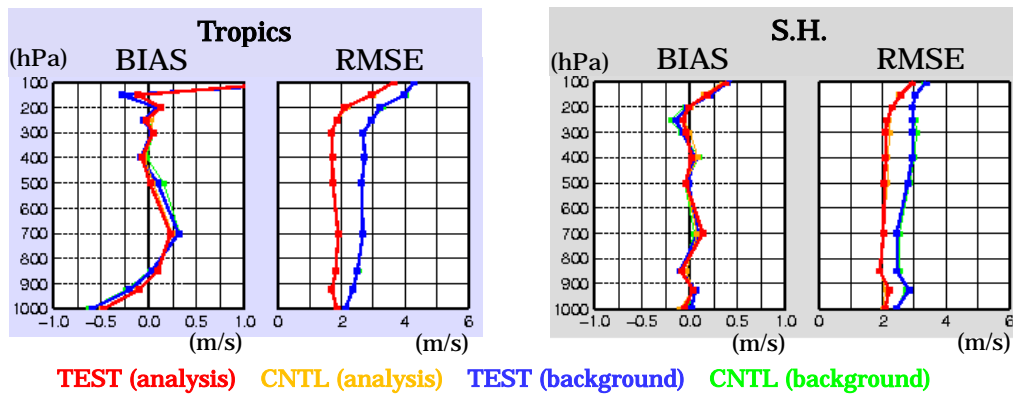


Figure 1: Wind speed error profiles of analysis and background against radio-sonde observation in the tropics (left panel) and the Southern Hemisphere (right panel). BIAS (right) and RMSE (left) are shown in each panel. The red, orange, blue and green lines represent analysis for TEST, analysis for CNTL, background for TEST and background for CNTL, respectively.

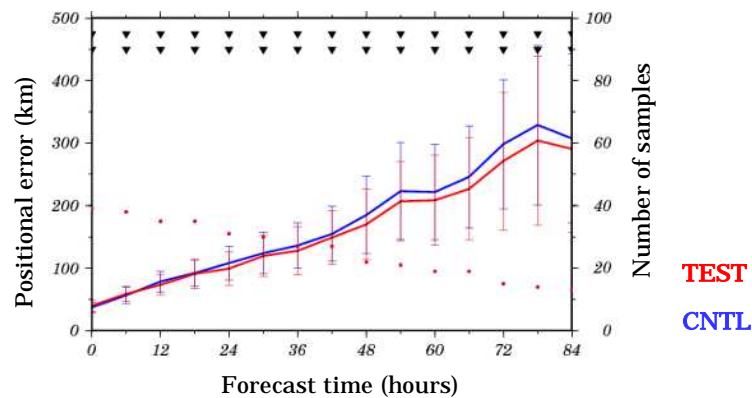


Figure 2: Average typhoon track forecast errors for August 2013. The red and blue lines represent the positional errors of TEST and CNTL, respectively. Red dots indicate the number of cases included in the statistics. The error bars represent a 95% confidence interval.

# Observing Simulation System Experiment (OSSE) of Spaceborne Doppler Wind Lidar

<sup>\*1,2</sup>Kozo OKAMOTO, <sup>2</sup>Shoken ISHII, <sup>2</sup>Philippe BARON,  
<sup>1</sup>Toshiyuki ISHIBASHI, and <sup>1</sup>Taichu TANAKA

1. Meteorological Research Institute (MRI) of Japan Meteorological Agency (JMA)

2. National Institute of Information and Communications Technology (NICT)

\*E-mail: kokamoto@mri-jma.go.jp

## 1. Introduction and OSSE system

Spaceborne Doppler Wind Lidar (DWL) can provide global wind profile observations, which are significant for improving numerical weather prediction. To assess the quantitative impact of DWL, we have been developing the OSSE system and a full-scaled lidar simulator called ISOSIM-L (Integrated Satellite Observation SIMulator for a spaceborne coherent Doppler lidar; Baron et al., 2012). OSSE is based on the Sensitivity Observing System Experiment (SOSE) approach (Marseille et al., 2008). A pseudo-truth field is created in SOSE from adjoint sensitivity and existing observations. ISOSIM-L inputs the pseudo-truth winds and three-dimensional cloud and aerosol fields, and then calculates optical parameters of aerosols and clouds, backscattered power, and line of sight (LOS) wind speeds. The aerosol field is generated by the MRI global aerosol model MASINGAR (Model of Aerosol Species in the Global Atmosphere; Tanaka and Chiba, 2005), constrained by the pseudo-truth winds. Simulated LOS wind speeds are assimilated in the global data assimilation system based on the four-dimensional variational (4D-Var) scheme used in the operational system at JMA. Figure 1 presents the flow of OSSE.

## 2. Assimilation pre-processing of DWL wind data and preliminary results

ISOSIM-L estimates a LOS wind-speed error from a simulated signal-to-noise ratio after spatial averaging, for example, over 100 km along the satellite track and 0.5 to 2.0 km in the LOS direction. The error estimate is used for observation error assignment and quality control (QC) criteria in the data assimilation pre-processing. Figure 2 presents an example of the QC result in a data assimilation experiment. We assume a 2.0  $\mu\text{m}$  coherent DWL having two laser systems with a nadir angle of 35 degrees and orthogonal azimuthal angles of 45 and 135 degrees on a sun-synchronous polar-orbiting satellite crossing the equator around 1800 local time at 220 km altitude. Much data is rejected between 30 and 60 degrees latitude in the Southern Hemisphere as a result of a large error estimate due to few aerosols. In contrast, in the mid-latitudes of the Northern Hemisphere, many DWL LOS winds pass the QC with a relatively large amount of continental aerosols. In the upper troposphere of the Northern Hemisphere and Tropics, much DWL data is available due to strong backscattering from high clouds.

## 3. Plans

We are implementing several one-month data assimilation experiments including DWL LOS winds to validate the OSSE system. The second step of our development is evaluating the impact of DWL winds on forecast accuracy for various combinations of data assimilation parameters, such as observation errors and QC criteria, and DWL parameters such as lidar power and averaging distance. Comparison is also necessary using various OSSE approaches including a nature-run OSSE, helping us to carefully interpret OSSE results.

## References

Baron P., S. Ishii, K. Mizutani, T. Itabe, and M. Yasui, 2012: The Integrated Satellite Observation

SIMulator for a Coherent Doppler Lidar (ISOSIM-L). The proceedings of 30<sup>th</sup> Japanese laser sensing symposium, Kagawa, Japan, 6–7 September 2012, ISBN:978-4-9902916-6-2

Marseille, G. J., A. Stoffelen, and J. Barkmeijer, 2008a: Sensitivity observing system experiment (SOSE): A new effective NWP - based tool in designing the global observing system, *Tellus A*, **60**, 216–233.

Tanaka, T. Y. and Chiba, M., 2005: Global simulation of dust aerosol with a chemical transport model, MASINGAR, *J. Meteor. Soc. Japan*, **83A**, 255–278.

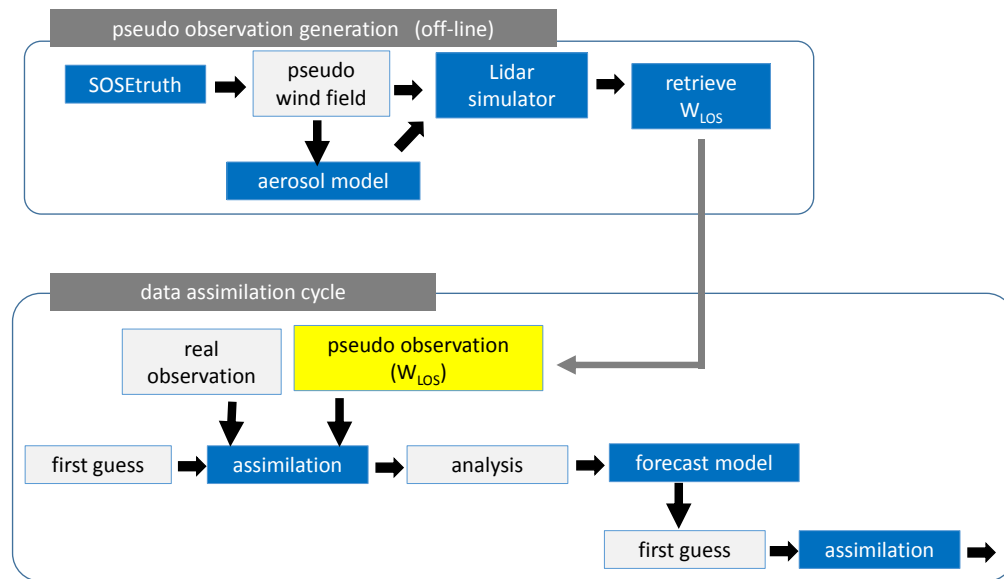


Fig.1. A flow of SOSE-OSSE. The top box is a DWL wind simulation step and the bottom box is a data assimilation step.

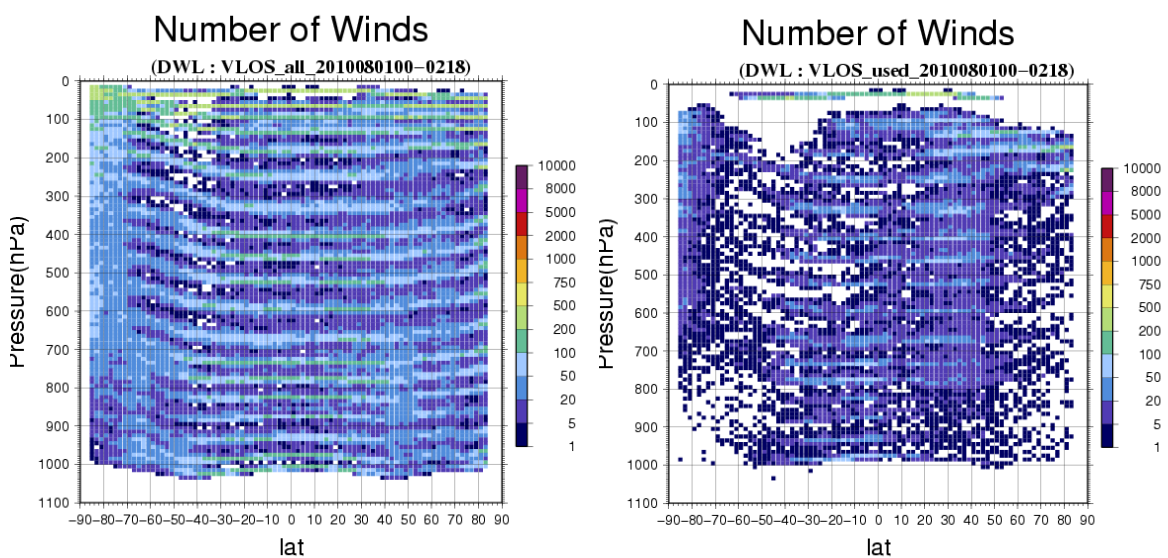


Fig.2. Zonally accumulated number in 2 degree x 20 hPa box from 1 to 2 August 2010 for DWL (left) before the QC (right) after QC.

# Development of a new Ensemble Variational Assimilation System in Meteorological Research Institute

\*Seiji ORIGUCHI, Kazumasa AONASHI, Takuya KAWABATA and Masaru KUNII  
Meteorological Research Institute, Tsukuba, Ibaraki, 305-0052, JAPAN  
E-mail; origuchi@mri-jma.go.jp

## 1. Introduction

The Japan Meteorological Agency (JMA) and the Meteorological Research Institute have already developed the data assimilation system based on an ensemble Kalman filter (EnKF; Fujita 2011). The system adopts the local ensemble transform Kalman filter (LETKF; Hunt et al. 2007) implemented with the JMA non-hydrostatic model (JMANHM; Saito et al. 2006). In the present study, the ensemble-based variational scheme (EnVar; Zupanski 2005, Zupanski et al. 2008, Liu et al. 2008) is newly additionally developed for an analysis step, which will facilitate the comparison between the EnKF and EnVar. Here, the newly developed EnVar is applied to the case of Typhoon Talas in 2011, and its performance is evaluated by single observation assimilation experiment. Although the system is based on the three-dimensional (3D) variational data assimilation, realistic analysis increments are produced through its flow-dependent background error estimates from ensemble forecasting. As an extension of the present configuration, a four-dimensional (4D) EnVar is currently being implemented, and it is currently being tested.

## 2. System of the developed EnVar

The cost function of the EnVar is written by the following formula, and the optimal analysis is derived from the minimization of the cost function.

$$J(\bar{\mathbf{x}}^a) = \frac{1}{2}[\bar{\mathbf{x}}^a - \bar{\mathbf{x}}^f]^T \mathbf{P}_f^{-1}[\bar{\mathbf{x}}^a - \bar{\mathbf{x}}^f] + \frac{1}{2}[\mathbf{H}(\bar{\mathbf{x}}^a) - \mathbf{y}]^T \mathbf{R}^{-1}[\mathbf{H}(\bar{\mathbf{x}}^a) - \mathbf{y}]$$

$$\begin{cases} \bar{\mathbf{x}}^a - \bar{\mathbf{x}}^f = \mathbf{P}_f^{1/2} \cdot \bar{\mathbf{w}}^a & \bar{\mathbf{w}}^a = [\bar{w}_1^a, \bar{w}_2^a, \dots, \bar{w}_N^a]^T \\ \mathbf{P}_f^{1/2} = [\mathbf{p}_1^f, \mathbf{p}_2^f, \dots, \mathbf{p}_N^f] = \frac{1}{\sqrt{N-1}} [\mathbf{x}_1^f - \bar{\mathbf{x}}^f, \mathbf{x}_2^f - \bar{\mathbf{x}}^f, \dots, \mathbf{x}_N^f - \bar{\mathbf{x}}^f] \end{cases}$$

$\mathbf{x}_i^f$  ; Ensemble forecast (i; member)     $\bar{\mathbf{x}}^f$  ; Ensemble mean  
 $\bar{\mathbf{x}}^a$  ; Analysis     $\bar{\mathbf{w}}^a$  ; Control variable  
 $\mathbf{P}_f$  ; Background error covariance     $\mathbf{R}$  ; Observation error covariance

Algorithm of the developed EnVar is shown in Fig. 1. The optimal analysis is estimated with the LBFGS method using the cost function and its gradient in ensemble space. Since the gradient vector and the Hessian matrix are calculated using the ensemble perturbation. Hence, the tangent linear and the its adjoint codes are not required in the EnVar. The square root of the background error covariance matrix with the flow-dependency is constructed by the ensemble perturbation.

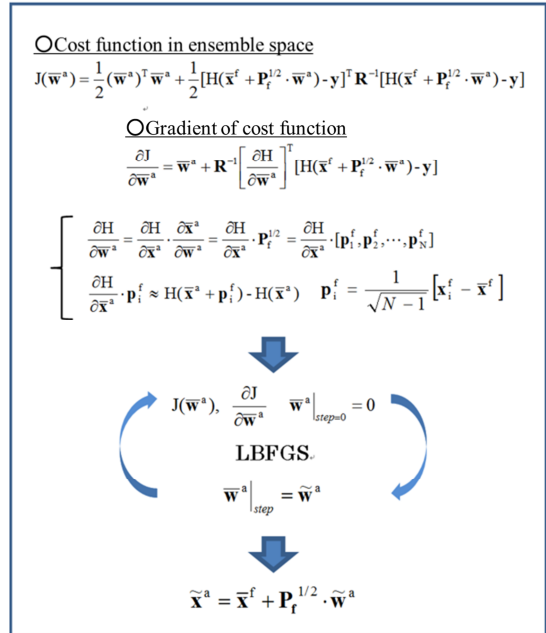


Fig. 1 Algorithm of the EnVar

### 3. Single observation assimilation experiment

First, the performance of the 3DENVar is evaluated by a single observation assimilation experiment for the case of Typhoon Talas. The wind velocity of pseudo observation is set to be two times larger than that of the first guess ( $U = -35.54 \text{ ms}^{-1}$ ,  $V = 45.68 \text{ ms}^{-1}$ ,  $Z = 5 \text{ km}$ ) at the northeast side of typhoon's central position. The observation error is set very small to emphasize the analysis increment ( $R_{\text{err}} = 0.5 \text{ m/s}$ ). As a result, positive increment is appeared along typhoon's circulation, and flow-dependent pattern is shown with a circulation enhancement (Fig. 2), suggesting that the wind data are assimilated appropriately.

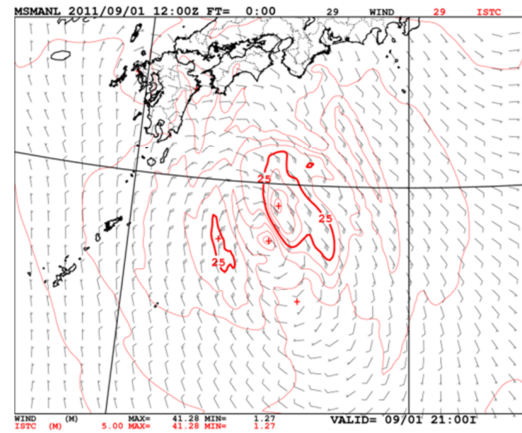
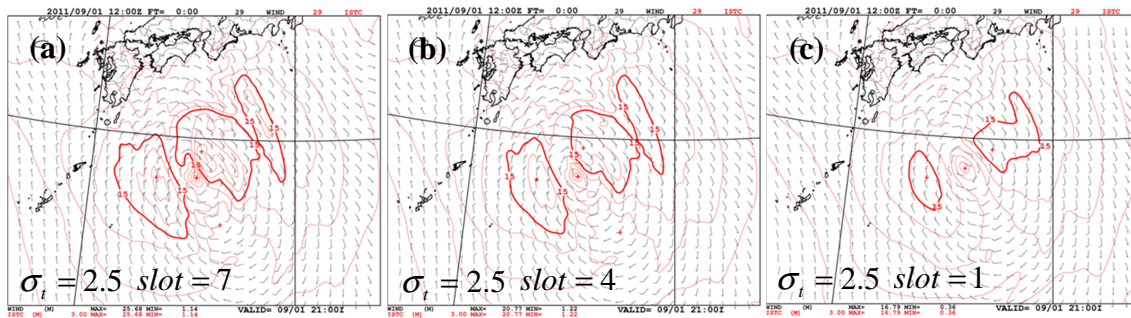


Fig. 2. Analysis increment (Wind, Height 5 km)

Next, temporal localization is implemented by the observation error by multiplying the reciprocal of the localization function. To see the effect of the temporal localization, sensitivity experiments are carried out in which a single observation is assimilated with different time intervals from the analysis. Figures 3a, 3b and 3c show the analyzed increments in which the pseudo observations were given at 0, 3 and 6 hours before the analysis time (corresponding slots are 7, 4 and 1, respectively). The increments became smaller with the increasing of the distance between observation and analysis times. These distributions indicate that the temporal localization worked effectively.



Figs. 3(a-c) Analysis increment (Wind, Height 5 km)  
Assimilation window of 6 hours is divided into 7 slots. Analysis slot is 7.

The performance of the 4DENVar which is implemented as an extension of the control variable is currently being tested for the same typhoon.

### References

- [1] Fujita, T., *NPD report*, **57**, 130-143 (2011) in Japanese
- [2] Hunt, B. R., E. J. Kostelich, and I. Szunyogh, *Physica D*, **230**, 112-126 (2007)
- [3] Liu, C., Q. Xiao, and B. Wang, *Mon. Wea. Rev.* **136**, 3363-3373 (2008)
- [4] Saito K., T. Fujita, Y. Yamada, J. Ishida, Y. Kumagai, K. Aranami, S. Ohmori, R. Nagasawa, S. Kumagai, C. Muroi, T. Kato, H. Eito and Y. Yamazaki, *Mon. Wea. Rev.* **134**, 1266-1298 (2006)
- [5] Zupanski, M., *Mon. Wea. Rev.* **133**, 1710-1726 (2005)
- [6] Zupanski, M., I. M. Navon, and D. Zupanski, *Quart. J. Roy. Meteorol. Soc.* **134**, 1039-1050 (2008)

### Acknowledgement

A part of this research has been funded by MEXT Strategic Programs for Innovative Research (SPIRE).

# Assimilation Experiments of MTSAT Rapid Scan Atmospheric Motion Vectors

Michiko Otsuka<sup>\*1</sup>, Masaru Kunii<sup>\*1</sup>, Hiromu Seko<sup>\*1</sup>, Kazuki Shimozi<sup>\*2</sup> and Masahiro Hayashi<sup>\*2</sup>

<sup>1</sup>Meteorological Research Institute, Japan Meteorological Agency

<sup>2</sup>Meteorological Satellite Center, Japan Meteorological Agency

E-mail: motsuka@mri-jma.go.jp

## 1. Introduction

The MTSAT-1R (Multi-functional Transport Satellite), a geostationary satellite of the Japan Civil Aviation Bureau (CAB) and the Japan Meteorological Agency (JMA), began rapid scan operations in 2011. It has been providing images of Japan and its neighboring area (latitude/longitude range from 20°N/120°E to 50°N/150°E) as frequently as five minutes during daytime in summer for the purpose of monitoring severe convective weather or volcanic ash plumes that could possibly affect the air traffic. The Meteorological Satellite Center (MSC) of JMA has produced Rapid Scan Atmospheric Motion Vectors (RS-AMVs), which are wind vectors derived from three consecutive rapid scan images tracking spatial distribution features of clouds and water vapor. RS-AMVs are expected to capture atmospheric motions in smaller space and time scale than hourly AMVs that are obtained from images at longer intervals currently in operationally use. The study intends to show the advantages of assimilating RS-AMVs in better forecasting mesoscale phenomena such as local heavy rainfall.

## 2. Outline of Experiments

Assimilation experiments utilizing RS-AMVs were performed over a heavy rainfall case that occurred in the western part of Japan on August 13<sup>th</sup> in 2012. The four-dimensional variational data assimilation system (JNOVA) with a resolution of 5 km in horizontal and 40 levels in vertical, based on JMA non-hydrostatic model (JMA-NHM), was used in the experiments. In the test experiment (TEST), RS-AMVs were assimilated at every ten minutes in a 3-hour timeslot window for nine hours during daytime (from 0000 to 0900 UTC), while other observations such as surface, upper-air, aircraft, satellite, wind profiler, radar, and GPS data were assimilated hourly. Then using the analysis at 09 UTC as initial values and JMA Global Spectral Model forecasts as boundary conditions, a 15-hour forecast was performed from 0900 UTC initial time with a resolution of 2 km (350 x 350 grid points) and 60 levels. On the other hand, RS-AMVs were not assimilated in the control experiment (CNTL), but a 15-hour forecast was conducted in the same manner.

## 3. Results

The convective cloud band corresponding to the synoptic front that stretched over the Japan Sea and its coast area was slowly moving to the south at 0000 UTC on August 13<sup>th</sup>. Five-minute interval rapid scan images clearly showed that the inflow bands of low cumulus clouds over the East China Sea off the west coast of Kyushu moved up toward the front from the south-west (Fig. 1). Associated with these cloud motions, south-westerly winds were obtained as lower AMVs in the area where the cumulus clouds were tracked, while many upper AMVs representing jet streaks were calculated in the vicinity of the front. Figure 2 gives the distribution of the upper and lower RS-AMVs that were assimilated during 0000 – 0900 UTC off the west of Kyushu, which indicates a divergence at upper levels (the red circle in the Fig. 2) and inflow at low levels. The analysis values

at 0900 UTC of TEST increased from those of CNTL in surface wind speed and convergence (Fig. 3 (a)) as well as in water vapor near surface level (Fig. 3 (b)) in the area mentioned above. These changes may result in the intensification of the front system over the Japan Sea and increase in amount of rainfall forecast at 1200 UTC off the coast of Chugoku and Kyushu (Fig. 3 (c)).

#### 4. Conclusion

Although the results are so far preliminary, RS-AMVS may have some positive impact on forecasts of the timing and the intensity of a heavy rainfall because of their high resolution and possibility to track clouds more accurately especially at low levels. In order to utilize RS-AMVs more effectively in Numerical Weather Prediction, there should be improvement in assimilation techniques for data quality control, data thinning or estimation of observational errors as well as development of AMV retrieval algorithms that is more suitably designed for high-resolution rapid scan observations.

#### Acknowledgement

This research was supported by JST, CREST.

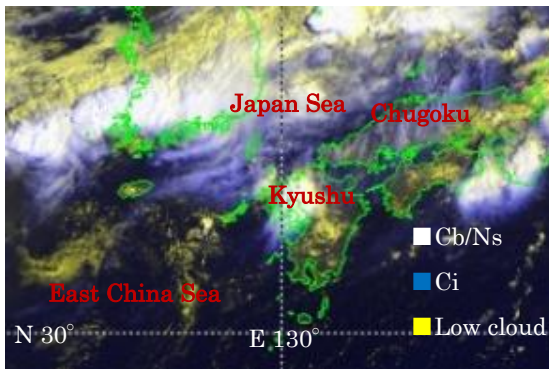


**Figure 1.** IR/VIS combined imagery by MTSAT at 0005 UTC on August 13<sup>th</sup> in 2012.

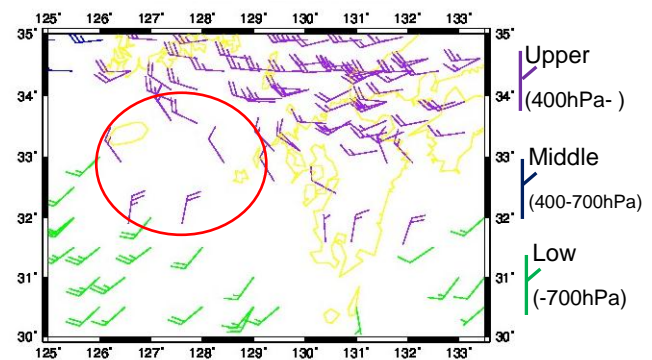
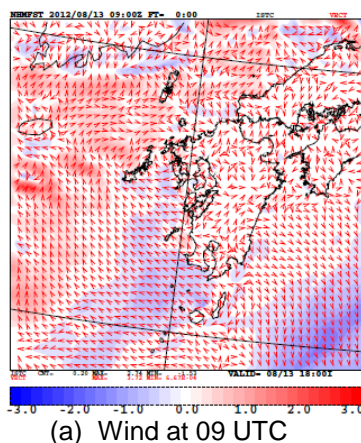
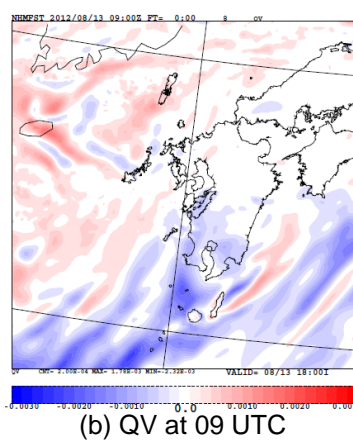


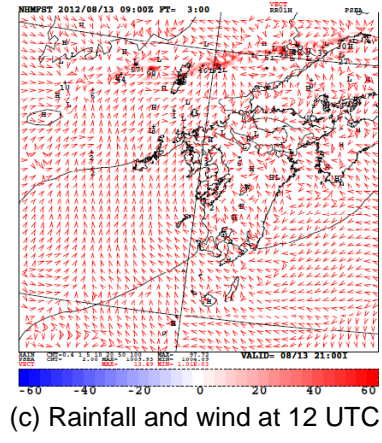
**Figure 2.** RS-AMVs assimilated in TEST (00-09 UTC). The red circle indicates a diversion spot in the upper-air.



(a) Wind at 09 UTC



(b) QV at 09 UTC



(c) Rainfall and wind at 12 UTC

**Figure 3.** Differences of analysis and forecast between TEST and CNTL (TEST minus CNTL) near surface level. (a) Analysis of wind speed [m/s] (color shading) and wind vector (arrows) at 09 UTC, (b) analysis of water vapor mixing ratio [kg/kg] (color shading) at 09 UTC, (c) forecast of rainfall [mm/h] (color shading) and wind vectors (arrows) at 12 UTC (FT=03).

# Data Assimilation Experiments of Refractivity Observed by JMA Operational Radar

\*Hiromu SEKO (MRI, JAMSTEC), Yoshihisa KIMATA (JMA),  
and Toshitaka TSUDA (Kyoto Univ./RISH)

## 1. Introduction

Radio waves, which are transmitted by Doppler radars and reflected from static structures (e.g. electronic power supply towers) are delayed by water vapor on paths between Doppler radars and static structures. If the delays of radio waves can be obtained from their phase data, refractivity - which is a function of water vapor and temperature - can be obtained from the delay data. This refractivity is expected to be useful in assimilating data for convection generations, because convergence of water vapor that generates convections is reproduced by assimilation of the refractivity. In this report, preliminary results of data assimilations, in which ‘temporal increments of refractivity (abbreviated to TIR, hereinafter)’ are used in producing initial conditions of numerical forecasts, will be presented.

## 2. Estimation methods of temporal increments of refractivity

In this report, phase data observed on 4<sup>th</sup> August 2008 by Tokyo radar of Japan Meteorological Agency (JMA) with the elevation angle of 0.0 degrees was used as assimilation data. It is difficult to estimate the absolute values of delays, because reflection points of radio waves, which are needed in the estimation of absolute wave numbers, cannot be determined. Then, ‘temporal increment of difference between the transmitted phase and the received phase’ (abbreviated to TIP) is used. The TIP, which is obtained by Radar observation, is the integrated value of TIR along the path of radio waves. The TIR, which will be used as assimilation data, is produced by making the difference of TIP in radial direction of Radar. The radio waves that are received by Radar are not only those reflected from static structures. It is necessary to remove the delays reflected from moving structures, such as trees and wind turbines. In Seko et al

(2009), the radio waves reflected from static structures were picked out from all reflected radio waves by using the temporal dispersion of TIP. Namely, radio waves, of which TIP fluctuated largely with time, were removed as ones reflected from moving structures. However, operational radars of JMA conduct volume scan observations and then the observation with the elevation angle 0.0 degrees, which is the most favorable elevation angle for the observation of static structures, was performed every 10 minutes. It is difficult to identify the radio waves reflected from static structures by using this intermittent data. Instead of temporal fluctuations of TIP, horizontal variations of TIP are used. Namely, (1) TIP is averaged over

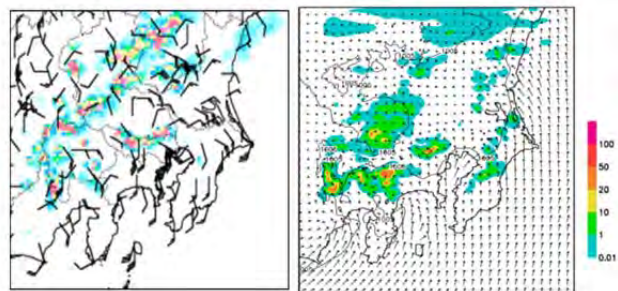


Fig.1 Observed distributions of rainfall region and horizontal wind at 16 JST (Left), and rainfall region and horizontal wind reproduced by the Inner LETKF at 15 JST (Right).

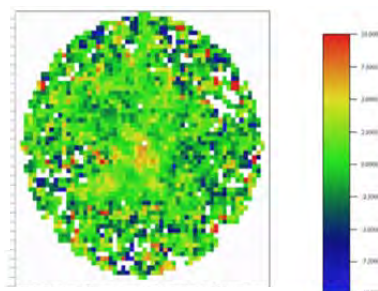


Fig. 2 Increment of refractivity from 1600 to 1610 JST.

small area, into which the Radar range is segmented. (2) The radio waves, of which temporal increment of refractivity is far from its areal average, are removed. After a few iterations of these procedures, the radio waves reflected from static structures are expected to remain. Though the threshold value used in identifying the moving structures in this study was determined by trial and error, it should be tuned because it might depend on atmospheric conditions.

### 3. Data assimilation methods and impact of refractivity

The system used in this experiment is a two-way nested system of LETKF (Seko et al. 2013). Outer LETKF, of which grid interval was 15 km, was performed from 09 JST 1<sup>st</sup> August to reproduce the mesoscale convergence, and the Inner LETKF was performed from 03 JST 4<sup>th</sup> to reproduce the convections. Conventional assimilation data of JMA was used by the outer and inner LETKFs, and refractivity data was added to the conventional assimilation data in the assimilation of the Inner LETKF. The interval of the inner LETKF's data slots is 10 minutes. We assumed that the analyzed distributions of 1500 JST are correct and obtained the refractivity distributions from 1510 JST to 1600 JST by adding the temporal increments of refractivity to this analyzed distribution of 1500 JST.

Figure 1 shows the rainfall regions observed by conventional radars and reproduced by the Inner LETKF. The rainfall region over the mountainous area surrounding the Kanto Plain was well reproduced. The rainfall region over the eastern part of the Tokyo Metropolitan area was also reproduced, though its generation time was 1 hour earlier than the actual one. Apart from these rainfall regions, weak rainfall regions that were not generated in reality extended in the eastern part of the Kanto Plain. Figure 2 is the observed temporal increment of refractivity at 1610 JST, which was estimated by using the aforementioned method. This distribution indicates that refractivity was increased where the rainfall region over the eastern part of the Tokyo Metropolitan area would be generated and decreased on its northeastern and eastern sides. When temporal increments of refractivity including one shown in Fig. 2 were assimilated, the fake rainfall regions became weaker (Fig. 3). The assimilation of the decreasing refractivity over the eastern part of the Kanto Plain reduced water vapor there, making the fake rainfall weaker. This result indicates that temporal increment of refractivity has the potential to improve the rainfall forecasts.

### References

- H. Seko, H. Yamauchi, O. Suzuki and K. Saito, Estimation of Temporal Variation of Refractive Index Using C-band Doppler Radar Equipped with Magnetron Transmitter, 2009, *SOLA*, 145-148.
- H. Seko, Tsuyuki, T., Saito, K., and Miyoshi, T., 2013: Development of a two-way nested LETKF system for cloud-resolving model. *Data Assimilation for Atmospheric, Oceanic and Hydrologic Applications (Vol. II)*, pp. 489-507.

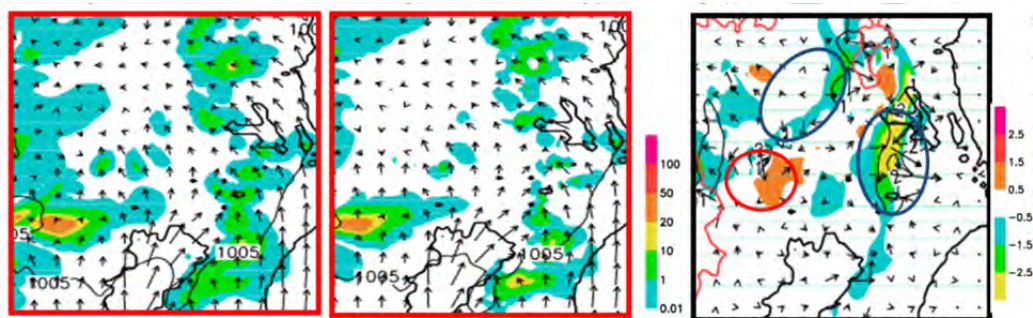


Fig. 3 Rainfall regions and horizontal wind at 16 JST reproduced by the Inner LETKF. (left) w/o refractivity, (center) with refractivity, and (right) increments caused by the refractivity data. Colored regions and contour indicate water vapor and temperature increments.

# The CNMCA (Italian National Meteorological Center) Operational LETKF Data Assimilation System

Lucio Torrisi<sup>a</sup> and Francesca Marcucci<sup>a</sup>

<sup>a</sup> CNMCA, Italian National Meteorological Center, Rome, Italy

The CNMCA short-range prediction system is based on the Ensemble Kalman Filter (EnKF) approach [1,2] for the data assimilation component and the COSMO regional model ([www.cosmo-model.org](http://www.cosmo-model.org)) for the prognostic one. In particular the Local Ensemble Transform Kalman Filter (LETKF [3]) scheme has been implemented at CNMCA, because it is easy to implement, intrinsically parallel and more efficient and flexible for nonlocal observations.

The operational implementation of the LETKF algorithm at CNMCA makes use of a 40+1 member ensemble based on the COSMO model. The COSMO model is integrated on the European Mediterranean region (COSMO-ME) at 10 km horizontal resolution on 45 model levels. A 6 hourly intermittent analysis cycle is implemented, making use of the observations available in a 6-h window centred at the analysis time. The observational dataset operationally ingested comprises 4D radiosonde ascents (RAOB), surface pressure observations from land and sea stations (SYNOP, SHIP, BUOY), manual and automatic aircraft observations, atmospheric motion vectors from Meteosat, European wind profilers, scatterometer winds from METOP/OceanSat2 and AMSU-A/MHS radiances from METOP and NOAA satellites. The CNMCA-LETKF data assimilation system is used to initialize the COSMO-ME model at the resolution of  $0.0625^\circ$  ( about 7 km). A schematic view of the operational NWP system is given in Fig.1.

## ***Lateral Boundary Conditions Perturbation***

Implementation of a limited-area ensemble Kalman filter (EnKF) needs a suitable way to perturb lateral boundary conditions. Usually a proper ensemble of boundary conditions can be provided by an EnKF on a larger domain (Global Ensemble Value method) or can be obtained by perturbation around a deterministic estimate using assumed spatial and temporal covariance relationships. We choose to follow an hybrid solution: the ensemble of boundary conditions is obtained perturbing the most recent available IFS deterministic forecast making use of the ECMWF-EPS. The 40 EPS members are randomly chosen and the perturbation of each one with respect to their mean is added to the IFS deterministic forecast.

The Sea Surface Temperature (SST) is also climatologically perturbed using the differences of the IFS SST analysis from the ECMWF operational archive.

## ***Model and sampling error treatment***

A multiplicative and additive covariance inflation has introduced to ameliorate sampling errors due to small ensemble size and also to account for model errors in assimilating real observations.

The method proposed in [4], the so called “relaxation-to-prior spread” (RTPS), has been tested and implemented, because the successful results with respect to the “3-dimensional adaptive-temporally smoothed multiplicative inflation” [5]. A clear improvement has been obtained when the RTPS was used in combination with an additive inflation technique.

In the first version of the CNMCA-LETKF system, based on HRM model, a climatological additive noise were implemented. Climatological additive inflation has the technical disadvantage to require an “enough” long period of 36/48h forecasts (it needs to re-run the model or to interpolate old runs to the new resolution), for these reasons an alternative method based on ECMWF-EPS forecast has been chosen, when we moved to COSMO model. The difference between EPS ensemble forecasts valid at the analysis time is computed and interpolated on the COSMO grid. The mean difference is then removed to yield a set of perturbations that are globally scaled and used as additive noise.

Recently, an adaptive flow-dependent additive inflation has been implemented and

experimentally tested. The perturbations are derived by a suitable scaling of the “zero-mean” differences of lagged CNMCA-LETKF ensemble forecasts giving a self-evolving and flow-dependent additive noise. A small positive impact has been found at second day forecast, probably because this additive error has a component that projects onto the growing forecast structures. The use of SPPT (Stochastic Physics Perturbation Tendencies) scheme is also under testing.

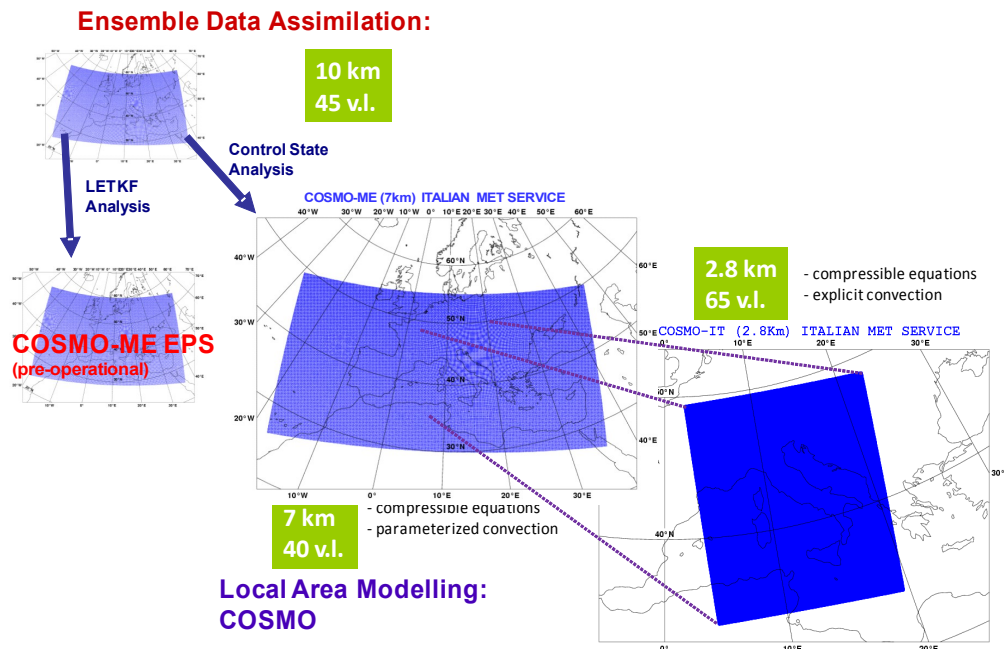


**Fig.1:** Schematic view of the operational CNMCA-NWP system.

## References

- [1] Bonavita M, Torrisi L, Marcucci F. 2008. The ensemble Kalman filter in an operational regional NWP system: Preliminary results with real observations. *Q. J. R. Meteorol. Soc.* 134, 1733-1744.
- [2] Bonavita M, Torrisi L, Marcucci F. 2010. Ensemble data assimilation with the CNMCA regional forecasting system. *Q. J. R. Meteorol. Soc.* 136, 132-145.
- [3] Hunt, B. R., E. Kostelich, I. Szunyogh. “Efficient data assimilation for spatiotemporal chaos: a local ensemble transform Kalman filter”, *Physica D*, 230, 112-126, 2007
- [4] Whitaker, J. S., T. M. Hamill ” Evaluating Methods to Account for System Errors in Ensemble Data Assimilation”. *Mon. Wea. Rev.*, 140, 3078–3089, 2012
- [5] Li, H., E. Kalnay, and T. Miyoshi, 2009: Simultaneous estimation of covariance inflation and observation errors within ensemble Kalman filter. *Q. J. R. Meteor. Soc.*, **135**, 523-533.

# Introduction of LEO-GEO and AVHRR Polar Atmospheric Motion Vectors into JMA's Operational Global NWP System

Koji Yamashita

Numerical Prediction Division, Japan Meteorological Agency  
e-mail: kobo.yamashita@met.kishou.go.jp

## 1. Introduction

LEO-GEO atmospheric motion vectors (AMVs) are derived in the latitudinal zone from approximately 60° to 70° using composite satellite imagery (a combination of geostationary (GEO) and polar-orbit (LEO) images) because there is a gap in coverage between middle-latitude and tropic AMVs derived from GEO images and those for polar regions derived from LEO images (Lazzara et al. 2014). LEO-GEO AMVs have been produced by the Cooperative Institute for Meteorological Satellite Studies (CIMSS) since November 2010. AVHRR (Advanced Very High Resolution Radiometer) polar AMVs (AVHRR AMVs) are estimated using AVHRR sequential images for areas over polar regions, and have been produced by CIMSS since 2006 (Key et al. 2008). The National Environmental Satellite, Data, and Information Service (NESDIS) of the National Oceanic and Atmospheric Administration (NOAA) has also been producing such AMVs on an operational basis since 2009. A specific quality control (QC) system was created to enable the use of LEO-GEO AMVs and AVHRR AMVs (the new AMVs) in operational global four-dimensional variational data assimilation (4D-VAR) on the NWP system (GSM-DA). Three-month observing system experiments (OSEs) for these new AMVs were performed using GSM-DA with the QC system in the summer and winter of 2012.

## 2. Characteristics of the new AMV data

The qualities of the new AMVs were evaluated statistically against the first-guess of the GSM-DA. Figure 1 shows a normalized histogram of the difference between their wind speeds and first-guess (O-B) data for the Northern Hemisphere (NH) in September 2011. These were compared with O-B data from CIMSS Moderate Resolution Imaging Spectroradiometer (MODIS) Terra AMVs, which are already assimilated in the operational GSM-DA. As shown in Fig. 1, the histograms of O-B for NH AMVs exhibit Gaussian distribution, and those for other regions have the same characteristics (not shown). The standard deviation (STD) of the O-B is 0.5 – 1.0 m/s larger than the MODIS Terra AMV values. The new AMVs have a negative bias against the first guess as with MODIS Terra AMVs. These AMVs are expected to increase the volume of such vectors available and to improve coverage poleward of 50° (Fig. 2).

## 3. QC for the new AMV data and OSEs

Development of the QC system for the new AMVs was based on the results outlined in Section 2. In this system, new AMVs with statistically large negative biases and STDs are rejected in pre-processing on the NWP system. The criteria settings for rejection of the new AMVs are the same as those for operational assimilated AMVs. The specific criteria for O-B STDs are 5 m/s above 400 hPa, 4 m/s from 400 to 700 hPa, and 2 m/s below 700 hPa. The other criterion setting for the O-B mean error is a level below 2 m/s (Yamashita 2008). QC settings are detailed on the NWP SAF AMV monitoring page<sup>1</sup>.

OSEs were performed to evaluate the impact of the new AMVs using GSM-DA. Global 4D-VAR data assimilation cycles were run every six hours, and 264-hour forecasts were executed from 12 UTC using the operational global spectral model (JMAGSM), which is a hydrostatic spectral model with a horizontal resolution of about 20 km (the resolution of the inner model for GSM-DA is about 55 km) and 60 vertical layers with the top level at 0.1 hPa. The OSE periods were from December 2011 to February 2012 (winter 2012) and from July to September 2012 (summer 2012). The terms TEST and CNTL are used to refer to the experiments with and without assimilation of the new AMVs, respectively. OSE results were compared to those of TEST against CNTL. Operationally

---

<sup>1</sup> [http://research.metoffice.gov.uk/research/interproj/nwpsaf/satwind\\_report/amvusage/jmamodel.html](http://research.metoffice.gov.uk/research/interproj/nwpsaf/satwind_report/amvusage/jmamodel.html)

assimilated observations, including GEO AMVs and MODIS AMVs, were used in both experiments.

#### 4. OSE results

Figure 3 shows the normalized root mean square error (RMSE) difference of the u-component wind in the first-guess and analysis field against aircraft observation in global area for summer 2012. The new AMVs bring reduced RMSEs between 300 and 600 hPa. The first-guess and analysis values of major components (wind, temperature and specific humidity) are generally improved against conventional and satellite observations (not shown). Figure 4 shows the normalized RMSE difference between forecasts covering periods from one to eleven days at 500 hPa geopotential height and wind vectors at 250 hPa for summer 2012. Significant positive impacts are seen until three-day forecasts, especially in the tropical and Southern Hemisphere, reaching up to 1 – 2% on average for summer 2012. Similar impacts on other physical elements and heights are also seen as described previously. Positive impacts were seen on typhoon track forecasts in the forecast period from 36 to 66 hours for summer 2012 (Fig. 5). Positive impacts were also seen for winter 2012 (not shown).

Based on these OSE results, the new AMVs were introduced into JMA's operational NWP system on 1 July, 2013.

#### References

- Key, J., D. Santek, C. S. Velden, J. Daniels and R. Dworak, 2008: The Polar Wind Product Suite. *Proc. 9th Int. Winds Workshop*, Annapolis, Maryland, USA, EUMETSAT. (Available online at <http://cimss.ssec.wisc.edu/iwwg/workshop9/index.html>)
- Lazzara, M. A., R. Dworak, D. A. Santek, B. T. Hoover, C. S. Velden and J. R. Key, 2014: High-latitude Atmospheric Motion Vectors from Composite Satellite Data. *Journal of Applied Meteorology and Climatology*, **53**, 534 – 547.
- Yamashita, K., 2008: Upgraded Usage of Atmospheric Motion Vectors from Geostationary Satellites in the Operational Global and Meso-Scale 4D-Var Assimilation System at JMA, *Proceedings of 9th IWW*, USA.

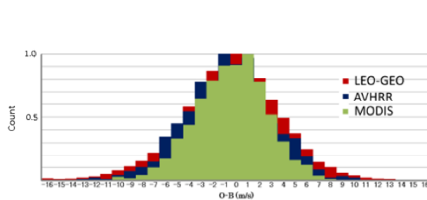


Figure 1. O-B normalized histograms of polar AMVs at levels above 400 hPa in the Northern Hemisphere (poleward of 20°N) for September 2011. The red, blue and green bars correspond to LEO-GEO, AVHRR in NOAA-18 and MODIS Terra AMVs, respectively.

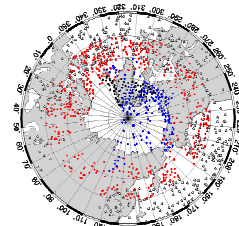


Figure 2. Polar AMVs used in the North Pole region in JMA's NWP system at 00 UTC on September 4, 2012. The blue dots are for AVHRR AMVs, and the red dots are for LEO-GEO AMVs.



Figure 3. Normalized RMSE difference between u-component wind in the first-guess (red line) and analysis (dashed red line) fields against aircraft observation over the globe from July to September 2012.

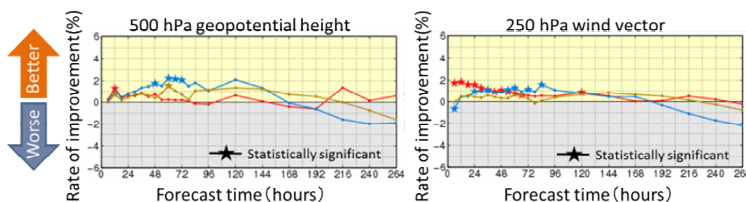


Figure 4. Normalized RMSE differences between forecasts covering periods from 1 – 11 days at 500 hPa geopotential height and 250 hPa wind vectors from July to September 2012. Positive values indicate better scores. The brown, red and blue lines show forecast improvement rates for the Northern Hemisphere (poleward of 20°N), tropic (20°S – 20°N) and Southern Hemisphere (poleward of 20°S) regions, respectively. The star plots indicate statistical significance.

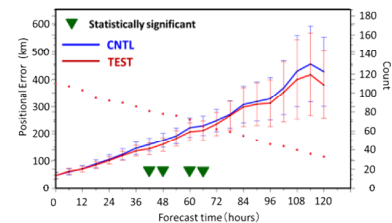


Figure 5. Average typhoon track forecast errors from July to September 2012. The red line is for TEST values, the blue line is for CNTL values, and the red dots are sample data numbers. The error bars represent a 95% confidence interval.

# The Impact of NASA TERRA MISR Atmospheric Motion Vector Assimilation into JMA's Operational Global NWP System

Koji Yamashita

Numerical Prediction Division, Japan Meteorological Agency  
e-mail: [kobo.yamashita@met.kishou.go.jp](mailto:kobo.yamashita@met.kishou.go.jp)

## 1. Introduction

MISR is the Multi-angle Imaging SpectroRadiometer on board the National Aeronautics and Space Administration's (NASA) Terra satellite, and MISR Atmospheric Motion Vectors (AMVs) are produced by NASA's Jet Propulsion Laboratory (JPL) using the MISR Level 2 Cloud product (Muller et al. 2012). AMVs derived from the MISR instrument have several unique strengths that are especially relevant to NWP systems. First, the integrated height retrievals are insensitive to radiometric calibration and atmospheric temperature profiles, giving more accurate height assignment for AMVs. Second, the cameras capture motion over a period of 200 seconds, providing effective 17.6 km gridded resolution data. Finally, MISR provides good global coverage up to 85 degrees north and south of the equator (Muller et al. 2012).

This report outlines the results of comparing MISR AMVs against collocated first-guess values of the operational global NWP system (JMAGSM) run by the Japan Meteorological Agency (JMA). It also details the outcomes of observing system experiments (OSEs) assimilating these AMVs in operational global four-dimensional variational data assimilation (4D-VAR) on the NWP system (GSM-DA).

## 2. Characteristics of MISR AMV data

Table 1 shows statistics such as the number of AMV data and the mean deviation/standard deviation of AMV wind speed departure from first-guess values (O-B) for the period from March to May 2012. The AMV numbers in the table indicate that most data are distributed in the low vertical layers (LL, below 700 hPa) and have positive biases against first-guess values of JMAGSM in all layers. The AMVs in LL have larger O-B standard deviation (STD) values than those of geostationary satellite AMVs (GEO-AMVs)<sup>1</sup>. Figure 1 shows a normalized histogram of O-B for the same period. The histogram of O-B for AMVs in the Northern Hemisphere (NH) exhibits approximate Gaussian distribution, which is favorable for data assimilation. The O-B histograms for other regions indicate the same characteristics as those of the Northern Hemisphere (not shown). The spatial correlation distance of O-B is longer than that of GEO-AMVs (e.g., MTSAT visible AMVs) in LL (Fig. 2). The O-B data for layers above 700 hPa has the same characteristics as those observed in Fig. 2 (not shown).

## 3. OSEs of MISR AMV data

OSEs were performed to evaluate the impacts of MISR AMVs using GSM-DA. Global 4D-VAR data assimilation cycles were run every six hours, and 264-hour forecasts were executed from 12 UTC using JMAGSM, which is a hydrostatic spectral model with a horizontal resolution of about 20 km (as opposed to the 55 km resolution of the inner model for GSM-DA) and 60 vertical layers with the top at 0.1 hPa. The OSE target period was July 2012.

Large differences were observed in the OSEs between the test without MISR AMV (CNTL) and that with MISR AMV (TEST). The AMV heights were converted from geometric heights to pressure levels with the assumption of International Civil Aviation Organization (ICAO) standard atmospheric conditions. MISR AMVs were thinned in  $1.5^\circ \times 1.5^\circ \times 100$  hPa horizontal-vertical boxes, and the minimum horizontal distance was set as 150 km. The thinning settings here were the same as those for polar AMVs. The quality control (QC) system adopted was the same as that indicated for GEO-AMVs on the NWP SAF AMV monitoring page<sup>2</sup> as a first step.

## 4. OSE results

---

<sup>1</sup> The STD of GEO-AMVs in LL is generally within 2 m/s.

<sup>2</sup> [http://research.metoffice.gov.uk/research/interproj/nwpsaf/satwind\\_report/amvusage/jmamodel.html](http://research.metoffice.gov.uk/research/interproj/nwpsaf/satwind_report/amvusage/jmamodel.html)

Figure 3 shows differences in the mean analyzed field for 700 hPa geopotential heights between TEST and CNTL. Large differences are observed all over the globe, especially at around 700 hPa. The number of assimilated MISR AMV data per analysis is approximately 1% against the whole body of input data. Figure 4 shows the normalized RMSE difference from one-day to eleven-day forecasts for July 2012. Although negative impacts are seen on two-day forecasts (especially in the tropics (EQ) and the Southern Hemisphere (SH)), positive impacts are seen on three-day forecasts in the Northern Hemisphere (NH).

The improvement of AMV coverage is contributing to the positive impact for the forecast skills in NH. The degraded forecasts seen for EQ and SH may stem from large observation error correlations or a positive bias of observation data against first-guess values as described in Section 2. Further research is required regarding the usage of MISR AMVs and other AMVs.

### Acknowledgements

The author is grateful to Dr. Kevin Mueller of the Jet Propulsion Laboratory at NASA for his technical support on MISR AMVs.

### References

Muller, K., M. Garay, C. Moroney and V. Jovanovic, 2012: MISR 17.6 km gridded cloud motion vectors: overview and assessment, *Proceedings of 11th IWW*, Auckland, Feb. 20 – 24.

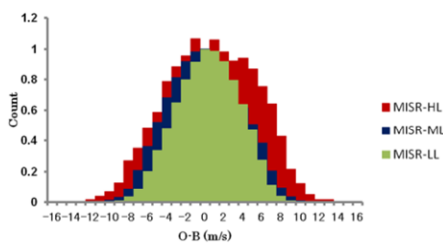


Figure 1. O-B histogram of MISR AMVs for the Northern Hemisphere (poleward of 20°N) during the period from March to May 2012. The red, blue and green bars correspond to the layers above 400 hPa (HL), from 400 to 700 hPa (ML) and below 700 hPa (LL), respectively.

	Count	ME (m/s)	STD (m/s)
NH-HL	9460	0.63	4.62
NH-ML	88987	-0.06	3.69
NH-LL	883638	0.29	3.26
EQ-HL	80495	0.32	4.72
EQ-ML	179916	0.52	3.43
EQ-LL	718210	0.77	3.10
SH-HL	9287	1.02	5.19
SH-ML	99164	0.35	3.96
SH-LL	526174	0.05	3.39

Table 1. Numbers of data (Count), mean errors (ME) and standard deviations (STD) for MISR AMVs. NH, EQ and SH represent the Northern Hemisphere (poleward of 20°N), the tropics (20°S – 20°N) and the Southern Hemisphere (poleward of 20°S), respectively. The other legend details are the same as those in Fig. 1.

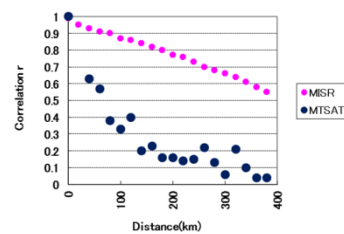


Figure 2. Spatial O-B error correlation coefficients for distance in MISR AMVs (pink plots) and MTSAT visible AMVs (blue plots) in the layer below 700 hPa for May 2012.

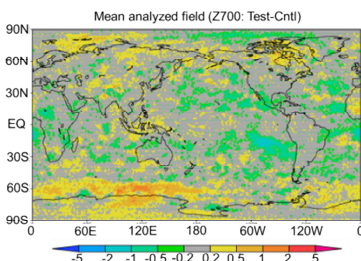


Figure 3. Mean analyzed field differences between TEST and CNTL at 700 hPa geopotential height for July 2012.

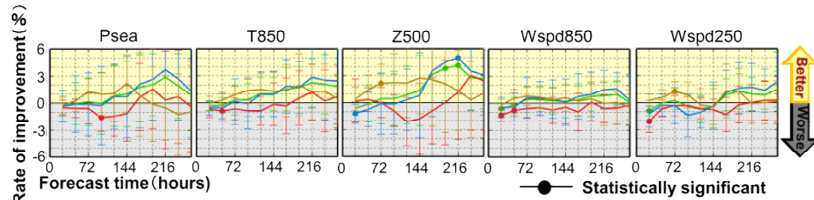


Figure 4. Forecast improvement rates with regard to RMSEs for 1 – 11-day forecasts for July 2012. The graph labeled Psea corresponds to surface pressure, T850 corresponds to 850 hPa temperatures, Z500 corresponds to 500 hPa geopotential heights, Wspd850 corresponds to 850 hPa wind speeds and Wspd250 corresponds to 250 hPa wind speeds. Positive values represent better scores. The green, brown, red and blue lines show forecast improvement rates for the global, Northern Hemisphere (poleward of 20°N), tropic (20°S – 20°N) and Southern Hemisphere (poleward of 20°S) regions, respectively. The error bars represent a 95% confidence interval.

# Doppler radar radial wind assimilation for the tornado outbreak on May 6, 2012

\*<sup>1</sup>Sho YOKOTA, <sup>1</sup>Masaru KUNII and <sup>2</sup>Hiromu SEKO

<sup>1</sup>Meteorological Research Institute, <sup>2</sup>Meteorological Research Institute/JAMSTEC

## 1. Introduction

A strong tornado with F3 scale was generated in Tsukuba City on May 6, 2012. It moved northeastward over the Kanto Plain, and caused serious damage. Besides the Tsukuba tornado, two tornadoes were observed a few ten kilometers north of the Tsukuba tornado. Tsukuba tornado passed 15 km north of the Meteorological Research Institute (MRI), and the lower vortex associated with the tornado, as well as its precipitation areas, was well captured by the Doppler radar of the MRI. Although data assimilation of the high-resolution data, such as Radar data, is important to reproduce small-scale phenomena like tornadoes in the numerical models, it has not been performed in this case yet. In this study, Doppler wind data observed by the MRI-Radar were assimilated with an ensemble Kalman filter and the impact of the assimilation of Doppler wind data was evaluated.

## 2. Experimental design

In this study, a Nested Local Ensemble Transform Kalman Filter (Nested-LETKF) system was used with 12 ensemble members. Figure 1 shows the outline of the system. In Outer-LETKF, horizontal grid interval is 15 km and hourly observation data were assimilated with 6 hour intervals. In Inner-LETKF, horizontal grid interval is 1.875 km and the data obtained every 10 minutes were assimilated with 1 hour intervals. To assess the impact of the Doppler wind observations, two experiments were performed. The first one is "CTL" experiment, in which conventional observations that are used in the Japan Meteorological Agency (JMA) operational model were assimilated in both Outer- and Inner-LETKF. Another is "VR" experiment, in which the Doppler wind observed by MRI-Radar was added to the assimilation data of Inner-LETKF. The Doppler wind data used for VR were ones with the elevation angles less than 5.0 degrees and with the horizontal resolutions of about 2.5 km. Other settings of VR were the same as CTL. After the data assimilation experiments, downscaling experiments with the grid interval of 350 m were carried out in VR and CTL from the analyzed fields of 13 members (12 perturbations and one analysis) of 10:00 JST on May 6, 2012.

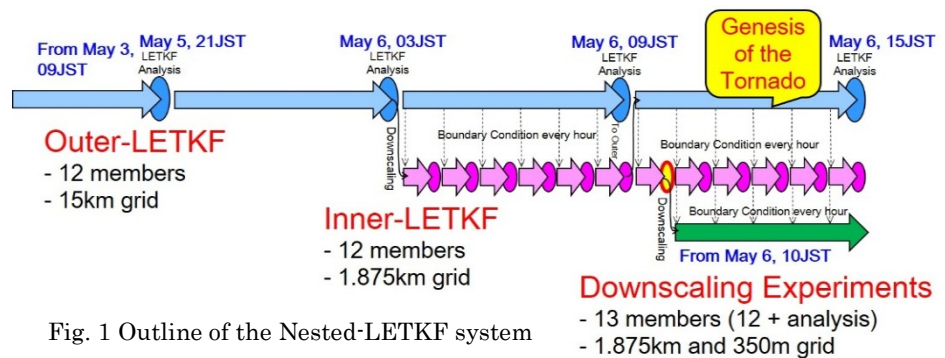


Fig. 1 Outline of the Nested-LETKF system

## 3. Results and correlation analysis

In the downscaling experiments, two vortices were formed in both VR and CTL. Figure 2 and 3 show the maximum velocity and the path of the southern vortex in these experiments, respectively. The path of the vortices were several kilometer north of the observed tornado in both VR and CTL. In VR, however, the southern vortex became stronger and passed about 2 km closer to the observed

tornado than those in CTL. To clarify what factors caused those differences, we focused on low level humidity at 20 m height ( $Q_v$ -low) and Storm Relative Helicity (SReH) at 10:00 JST. Figure 4 shows the difference of  $Q_v$ -low and SReH between VR and CTL. The correlations between  $Q_v$ -low and the maximum velocity of the vortex ( $V_{max}$ ) and between SReH and the latitude where the vortex existed when it passed 140E (L140) were also calculated by coarse-grained  $Q_v$ -low and SReH at 15 km resolution in the 13 members in VR (not shown).  $Q_v$ -low was larger at the south of the genesis point of the vortex in VR (Fig. 4, left), and it had positive correlation with  $V_{max}$  there. Therefore, larger  $Q_v$ -low at the south of the genesis point of the vortex made the  $V_{max}$  larger. On the other hand, SReH was larger at the north of the genesis point of the vortex in VR (Fig. 4, right), and it had negative correlation with L140 there. In addition, SReH was smaller at the south of the precipitation area in VR (Fig. 4, right), and it had positive correlation with L140 there. Therefore, increase of SReH at the north of the genesis point of the vortex and decrease of SReH at the south of the precipitation area caused that the path of the vortex shifted southward.

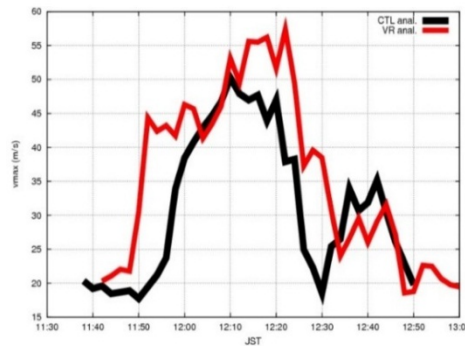


Fig. 2 The time series of maximum velocity of the south vortex at 20 m height in the downscaling experiment using analyses at 10:00 JST on May 6 as initial conditions (black: CTL, red: VR).

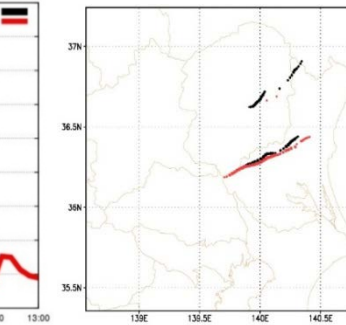


Fig. 3 The path of high relative vorticity areas at 20 m height ( $> 0.03 \text{ s}^{-1}$ ) in the downscaling experiment using analyses at 10:00 JST on May 6 as initial conditions (black: CTL, red: VR).

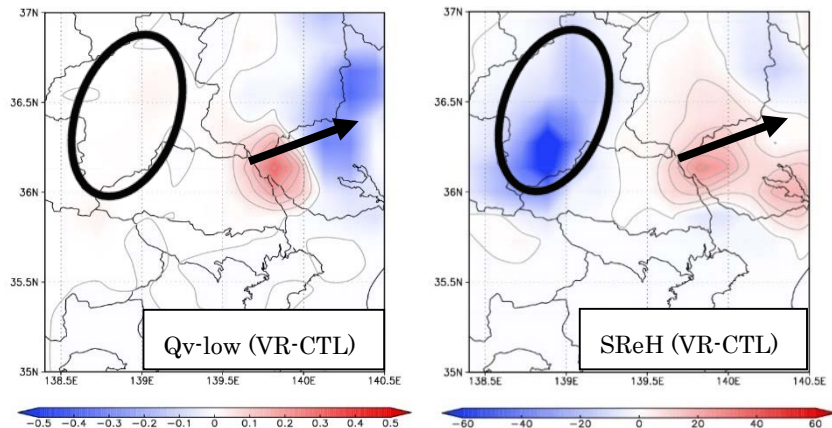


Fig.4 The difference of  $Q_v$ -low [ $\text{g kg}^{-1}$ ] (left) and SReH [ $\text{m}^{-2} \text{s}^{-2}$ ] (right) between the analyses of VR and CTL at 10:00 JST on May 6. Contour intervals are  $0.05 \text{ [g kg}^{-1}]$  and  $5 \text{ [m}^{-2} \text{s}^{-2}]$ , respectively, drawn only in positive. Ellipses show the precipitation region at 10:00 JST on May 6, and arrows show the path of the vortex in the downscaling experiments.

#### 4. Summary

The vortex became stronger and the path of the vortex became closer to the reality by the assimilation of Doppler wind data observed by the MRI-Radar. The wind speed of the vortex had correlation with  $Q_v$ -low at the south of the genesis point of vortices, and the location of the vortex had correlation with SReH at the north of the genesis point of vortices and the south of the precipitation area. Therefore, proper correction of these values by data assimilation of efficient observation data is important for better reproduction of the vortex.

#### Acknowledgements

The authors thank the 2<sup>nd</sup> Laboratory, Meteorological Satellite and Observation System Research Department, MRI for providing the Doppler radar data. This study was supported by "Strategic Programs for Innovative Research (SPIRE), Field 3" and "Tokyo Metropolitan Area Convection Study for Extreme Weather Resilient Cities (TOMACS)".